ORGANOMETALLICS

Article

pubs.acs.org/Organometallics

Five-Membered Heterocycles as Linking Units in Strongly Coupled Homobimetallic Group 8 Metal Half-Sandwich Complexes

Ulrike Pfaff,[†] Alexander Hildebrandt,[†] Marcus Korb,[†] Dieter Schaarschmidt,[†] Marco Rosenkranz,[‡] Alexey Popov,[‡] and Heinrich Lang*[,†]

[†]Institute of Chemistry, Inorganic Chemistry, Faculty of Natural Sciences, Technische Universität Chemnitz, D-09107 Chemnitz, Germany

[‡]Institute for Solid State Research, Department of Electrochemistry and Conducting Polymers, IFW Dresden, Helmholtzstraße 20, D-01069 Dresden, Germany

Supporting Information

ABSTRACT: The synthesis and characterization of a series of alkynyl half-sandwich complexes of type 2,5-((η^5-C_5H_5)(dppe)MC≡C)$_2$-^{c}C$_4$H$_2$E (E = O (**11**), S (**12**); M = Fe (**a**), Ru (**b**); dppe = 1,2-bis(diphenylphosphino)-ethane) are reported. The molecular structures of **11a** and **12a,b** in the solid state have been determined by single-crystal X-ray diffraction. The influence of different metals and the variation of the heterocyclic bridge on the electronic interactions between the terminal redox-active units in **11a,b** and **12a,b** was studied using electrochemical (cyclic and square wave voltammetry) and spectroelectrochemical (*in situ* UV−vis/NIR, ESR, and IR spectroscopy) methods and DFT calculations. Electrochemical studies demonstrated that mixed-valent species **11a,b**$^+$ and **12a,b**$^+$ exhibit high thermodynamic stabilities with respect to disproportionation (K_C values from 6.87×10^4 to 9.33×10^5). *In situ* spectroelectrochemical ESR and IR measurements display delocalization of the single electron between the metal centers M/M$^+$, revealing that within this setup five-membered heterocycles are well suited to promote intramolecular metal−metal interactions. Furthermore, the UV−vis/NIR spectra of mixed-valent **11a,b**$^+$ and **12a,b**$^+$ show intense, narrow, and nonsolvatochromic $\pi(d\pi) \rightarrow \pi^*(d\pi)$ absorptions in the NIR region with a high-energy shoulder. Both experimental and computational results suggest that at least two thermally accessible rotation conformers of the organometallic termini of **11a,b** and **12a,b** contribute to the electronic spectra of these compounds. One of the conformers can clearly be characterized as a delocalized class III system, while the other shows a more localized behavior.

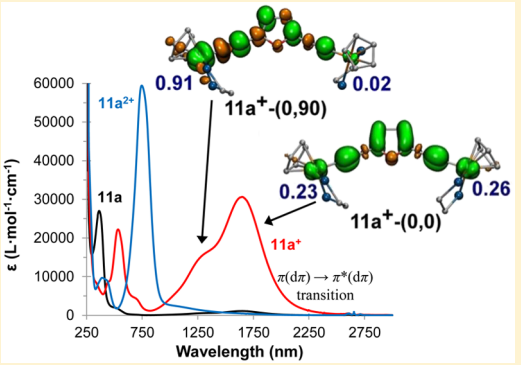

INTRODUCTION

The investigation of organometallic compounds bearing π-conjugated organic bridging ligands between transition metal atoms has increased significantly during the last 30 years.[1−3] In particular, alkynyl transition metal complexes are well studied, due to their high stability, π-conjugation, and rigid structure. They are well suited, for example, as models for "molecular wires"[4−7] and for the construction of nanoscale electronic devices.[8−12] Besides σ-complexes with *end-on* bonded alkynes, tweezer-type complexes with both σ- and π-coordination have been investigated, as they allow cooperative and synergistic effects between the metal centers.[13−15] Examples of alkynyl transition metal complexes are given by the works of, for example, Lapinte,[16−19] Low,[20−22] and Bruce.[23,24] Besides bridges solely built of alkyne chains,[25−28] other organic linkers such as benzene,[1,21,29,30] naphthalene,[1,31] anthracene,[1,17,32] bipyridine,[16] 1,12-carbaborane,[33] cyanoacetylide,[24] dithia[3.3]-paracyclophane,[34] and biferrocene[19,35−37] have been introduced in alkyne-based "all-carbon" units. Hence, the influence of the chain length and the nature of the organic unit on the intramolecular electronic communication between the transition metals in homo- and heterobimetallic compounds were investigated. It could be shown that, as expected, larger alkyne bridges lead to a decrease of the electronic interaction between the metal centers. Organometallic half-sandwich building blocks, e.g., ML(PP) (L = Cp (= η^5-C_5H_5) or Cp* (= η^5-C_5Me_5); M = Fe, Ru, Os; PP = dppe, dppm (= 1,2-bis(diphenylphosphino)methane), $(PPh_3)_2$),[25,26,29,35] Mn(η^5-C_5H_4Me)(dmpe) (dmpe = 1,2-bis(dimethylphosphino)-ethane),[38] Mo(η^7-C_7H_7)(dppe),[29] Pt$(PR_3)_2$(Ar),[25] and ReCp*-(NO)(PPh_3),[39,40] are primarily used as redox-active termini, whereby a direct bond between the metal and the "all-carbon bridge" is present.

Recently, our research group focused on the electrochemical behavior of ferrocenyl-functionalized heterocycles[41−44] including furan,[45] thiophene,[45,46] pyrrole,[45,47,48] phosphole,[49] silole,[50] titanacyclopenta-2,3,4-triene,[51,52] and zirconacyclopentadiene.[51] On the example of a series of aromatic diferrocenyl heterocycles of type 2,5-Fc$_2$-^{c}C$_4$H$_2$E (Fc = Fe(η^5-C_5H_5)(η^5-

Received: February 6, 2015

DOI: 10.1021/acs.organomet.5b00104
Organometallics XXXX, XXX, XXX−XXX

Scheme 1. Synthesis of 5 and 6,[a] 9a,b, 10a,b, 11a,b and 12a,b

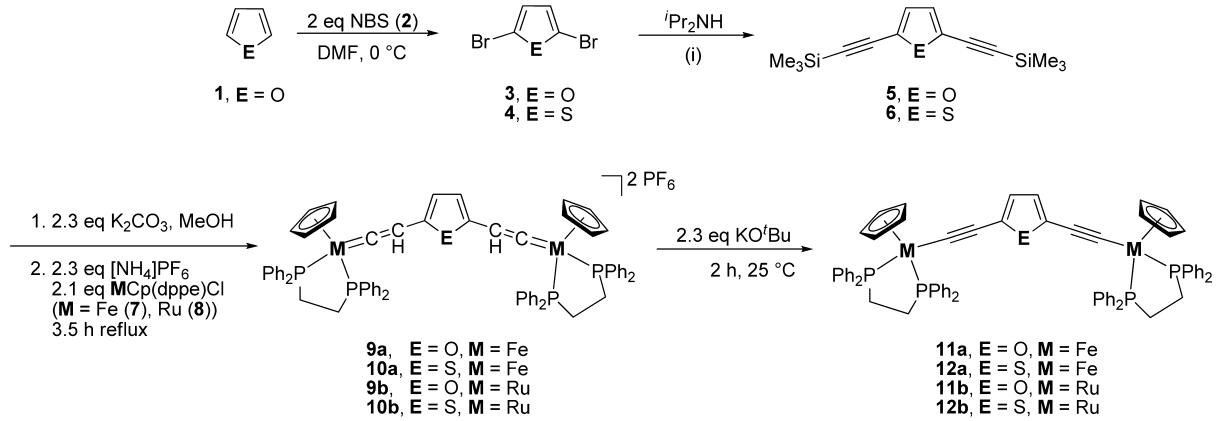

[a]Conditions: (i) 50 °C, 12 h, 6 mol % CuI, 0.5 mol % [PdCl$_2$(PPh$_3$)$_2$], 6 mol % PPh$_3$, 2.1 equiv trimethylsilyl acetylene. 2,5-Dibromothiophene (**4**) was purchased from chemical suppliers.

C$_5$H$_4$); E = O, S, NR; R = CH$_3$, C$_6$H$_5$, C$_6$H$_4$-4-NMe$_2$, C$_6$H$_4$-4-OMe, C$_6$H$_4$-4-Me, C$_6$H$_4$-3-F, C$_6$H$_4$-4-CO$_2$Et) a direct correlation between electrochemical and spectroscopic properties could be shown, due to similar molecular geometries (Fe–Fe distance, heterocycle) of the respective species.[45,47,48,53] The strength of the electronic coupling of the ferrocenyl/ferrocenium termini through the heterocyclic unit allowed the classification of these compounds as class II systems according to Robin and Day.[54]

The groups of Lapinte[55] and Lui[56] found for mixed-valent [2,5-(η^5-C$_5$Me$_5$)(dppe)MC≡C)$_2$-^{c}C$_4$H$_2$S]$^+$ (M = Fe, Ru) solvent-independent and narrow IVCT bands in NIR spectroelectrochemical studies. On the Mössbauer time scale the charge is delocalized on both metal centers M. IR spectroelectrochemistry revealed two distinct C≡C vibrations, characterizing them as class II/III borderline systems.[54] These investigations prompted us to combine the well-studied and electron-rich half-sandwich moieties M(dppe)Cp (M = Fe, Ru, Os; Cp = (η^5-C$_5$H$_5$)) with the five-membered heterocycles (*vide supra*) with a series of complexes of type 2,5-((η^5-C$_5$H$_5$)(dppe)MC≡C)$_2$-^{c}C$_4$H$_2$E (E = O, S). (Spectro)-Electrochemical methods and DFT calculations have been used to investigate the effect of various group 8 metals and heteroatoms on the electronic properties and intramolecular interactions of the latter type of compounds. Furthermore, the IR-active alkyne unit allowed to study the intramolecular electron transfer interactions on the IR time scale.

■ RESULTS AND DISCUSSION

Synthesis and Characterization. 2,5-Bis-(trimethylsilylethynyl)-functionalized heterocycles 2,5-(Me$_3$SiC≡C)$_2$-^{c}C$_4$H$_2$E (E = O (**5**), S (**6**)) were synthesized by the reaction of Me$_3$SiC≡CH with 2,5-Br$_2$-^{c}C$_4$H$_2$E (E = O (**3**), S (**4**)) under typical Sonogashira *C,C* cross-coupling conditions in diisopropylamine (Scheme 1). Compounds 2,5-((η^5-C$_5$H$_5$)(dppe)MC≡C)$_2$-^{c}C$_4$H$_2$E (E = O (**11**), S (**12**); M = Fe (**a**), Ru (**b**)) were obtained in a three-step "one-pot" reaction[55] based on the deprotection of **5** and **6** with K$_2$CO$_3$ in methanol, followed by treatment of the thus obtained 2,5-(HC≡C)$_2$-^{c}C$_4$H$_2$E species with MCl(dppe)Cp (M = Fe (**7**), Ru (**8**); Cp = (η^5-C$_5$H$_5$)), whereby the dissociation of the M–Cl bond is facilitated by the addition of 2.3 equiv of [NH$_4$]PF$_6$ to afford bis(vinylidene) compounds [2,5-((η^5-C$_5$H$_5$)(dppe)-M=C=CH)$_2$-^{c}C$_4$H$_2$E][PF$_6$]$_2$ (M = Fe, E = O (**9a**), S (**10a**); M = Ru, E = O (**9b**), S (**10b**)) (Scheme 1). *In situ* deprotonation of **9a,b** and **10a,b** with KO^{t}Bu produced **11a,b** and **12a,b**, respectively (Scheme 1, Experimental Section). After appropriate workup, compounds **11a,b** and **12a,b** were obtained as red (**11a** and **12a**) or pale green (**11b** and **12b**) solids in moderate yields (Experimental Section).

While the synthesis of **11a,b** and **12a,b** proceeded applying a straightforward synthesis protocol (Scheme 1), the use of OsBr(dppe)Cp did not afford the expected isostructural compounds 2,5-((η^5-C$_5$H$_5$)(dppe)OsC≡C)$_2$-^{c}C$_4$H$_2$E (E = O, S). Modification of the reaction conditions (different solvents, temperatures, reaction times, and bases) also did not result in the desired products.

Compounds **11a,b** and **12a,b** are less soluble in hexane, toluene, and diethyl ether; however, they show excellent solubility in dichloromethane and tetrahydrofuran. They are stable toward air and moisture in the solid state, while in solution they readily decompose when exposed to air, but are stable under an inert gas atmosphere. Characterization details for **11a,b** and **12a,b** (^{1}H, ^{13}C{^{1}H}, ^{31}P{^{1}H} NMR, IR spectroscopy, ESI-TOF mass spectrometry, and elemental analysis) are given in the Experimental Section and in the Supporting Information. The structures of **11a** and **12a,b** in the solid state are reported. In addition, (spectro)electrochemical measurements (*in situ* IR, UV–vis/NIR, ESR) were carried out to investigate the electronic properties of the mixed-valent species.

The ^{1}H NMR spectra of **11a,b** and **12a,b** show a characteristic singlet for the η^5-bonded cyclopentadienyl groups in the range 4.2–4.7 ppm, whereby the heavier ruthenium atom causes a shift to lower field. For the heteroaromatic moiety ^{c}C$_4$H$_2$E a singlet (**11a**, 5.75 ppm; **11b**, 5.70 ppm; **12a**, 6.29 ppm; **12b**, 6.26 ppm) for the protons in 3,4-position was detected. Due to the different electron density in the heterocycles, the signals of **12a,b** are shifted to lower field, when compared with the signals of the isostructural furan complexes.[57] In the ^{1}H NMR the aromatic phenyl protons of the dppe group are observed as triplets.[58]

Characteristic in the ^{13}C{^{1}H} NMR spectra of all complexes are the signals for the ethynyl units, which resonate at ca. 117 ppm (C≡C-M) and ca. 135 ppm (C≡C-^{c}C$_4$H$_2$E), respectively (Experimental Section). Noteworthy in the ^{13}C{^{1}H} NMR

DOI: 10.1021/acs.organomet.5b00104
Organometallics XXXX, XXX, XXX–XXX

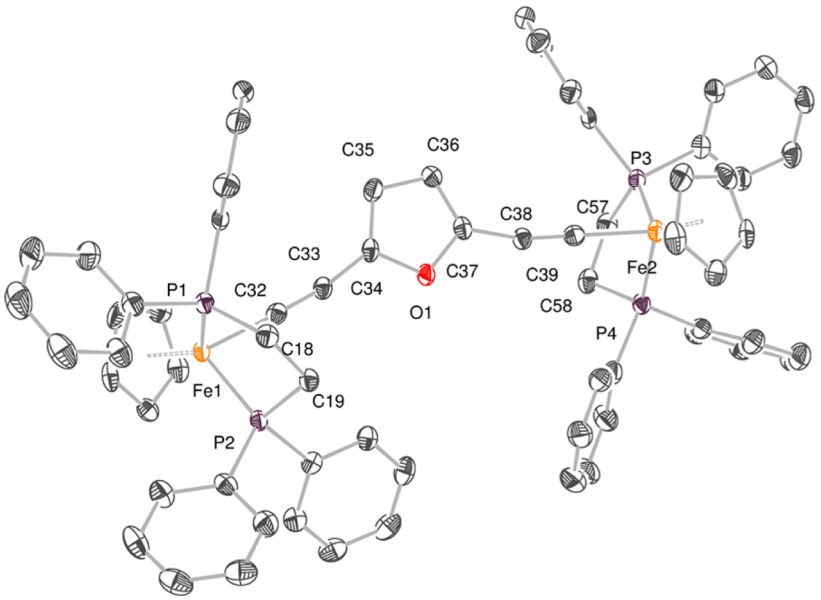

Figure 1. ORTEP diagram (50% probability level) of the molecular structure of **11a** with the atom-numbering scheme. Hydrogen atoms and solvent molecules have been omitted for clarity. Selected bond distances (Å), angles (deg), and torsion angles (deg): average D−Fe = 1.723, C34−C35 = 1.363(4), C35−C36 = 1.413(4), C36−C37 = 1.358(4), C34−O1 = 1.390(3), C37−O1 = 1.386(3), C33−C34 = 1.409(4), C32−C33 = 1.219(4), C32−Fe1 = 1.903(3), C37−C38 = 1.414(4), C38−C39 = 1.219(4), C39−Fe2 = 1.903(3), P1−Fe1 = 2.1564(7), P2−Fe1 = 2.1721(7), P3−Fe2 = 2.1620(7), P4−Fe2 = 2.1609(7); C35−C34−C33 = 131.7(2), C37−O1−C34 = 106.69(19), O1−C37−C38 = 120.3(2), C32−Fe1−P1 = 87.92(8), C32−Fe1−P2 = 84.77(8), C39−Fe2−P3 = 89.88(8), C39−Fe2−P4 = 86.31 (8), P1−Fe1−P2 = 85.83(3), P4−Fe2−P3 = 85.25(3), C33−C32−Fe1 = 178.0(2), C38−C39−Ru2 = 176.0(2); C34−C35−C36−C37 = −0.5(3), C38−C37−O1−C34 = 179.6(2), P1−C18−C19−P2 = −36.1(2), P3−C57−C58−P4 = −39.3(2), Fe1−C32−C33−C34 = −15(8), C37−C38−C39−Fe2 = −92(3), C18−P1−Fe1−C32 = −71.23(12), C58−P4−Fe2−C39 = 58.52(12) (D denotes the centroid of C_5H_5).

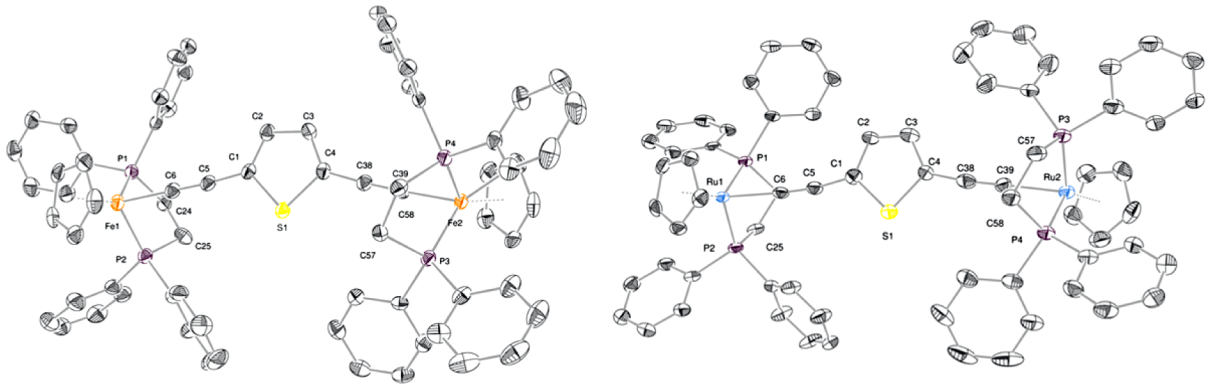

Figure 2. ORTEP diagram (50% probability level) of the molecular structures of **12a** (left) and **12b** (right) with the atom-numbering scheme. Hydrogen atoms and solvent molecules have been omitted for clarity. Selected bond distances (Å), angles (deg), and torsion angles (deg): Compound **12a**: average D−Fe = 1.713, C1−S1 = 1.748(3), C4−S1 = 1.749(4), C1−C5 = 1.418(5), C5−C6 = 1.229(5), C6−Fe1 = 1.883(3), P1−Fe1 = 2.1580(11), P2−Fe1 = 2.1600(11), P3−Fe2 = 2.1712(11), P4−Fe2 = 2.1590(10); C2−C1−C5 = 129.1(3), C2−C1−S1 = 109.9(2), C6−Fe1−P1 = 89.41(12), C6−Fe1−P2 = 85.52(11), C39−Fe2−P3 = 84.26(11), C39−Fe2−P4 = 88.30(10), P1−Fe1−P2 = 85.53(4), P4−Fe2−P3 = 85.77(4), C5−C6−Fe1 = 175.1(3), C38−C39−Fe2 = 177.6(3); C1−C2−C3−C4 = 0.6(5), C38−C4−S1−C1 = 179.7(3), P1−C24−C25−P2 = 39.8(3), P3−C57−C58−P4 = 32.3(3), C1−C5−C6−Fe1 = 66(8), C4−C38−C39−Fe2 = −32(13), C24−P1−Fe1−C6 = 74.93(16), C58−P4−Fe2−C39 = 68.97(16) (D = denotes the centroid of C_5H_5). Compound **12b**: average D−Ru = 1.896, C1−S1 = 1.742(4), C4−S1 = 1.752(4), C1−C5 = 1.433(5), C5−C6 = 1.200(5), C6−Ru1 = 2.020(4), P1−Ru1 = 2.2486(10), P2−Ru1 = 2.2595(9), P3−Ru2 = 2.2525(10), P4−Ru2 = 2.2472(10); C2−C1−C5 = 108.3(3), C2−C1−S1 = 108.3(3), P1−Ru1−C6 = 82.38(10), P2−Ru1−C6 = 92.96(10), C39−Ru2−P3 = 87.13(10), C39−Ru2−P4 = 84.54 (11), P2−Ru1−P1 = 82.91(3), P4−Ru2−P3 = 83.28(4), C5−C6−Ru1 = 174.2(3), C38−C39−Ru2 = 173.6(3); C1−C2−C3−C4 = 0.6(5), C38−C4−S1−C1 = −18.8(3), P1−C24−C25−P2 = −51.3(3), P3−C57−C58−P4 = 41.6(3), C1−C5−C6−Ru1 = −27(5), C4−C38−C39−Ru2 = −63(5), C24−P1−Ru1−C6 = 67.77(16), C58−P4−Ru2−C39 = −58.58(1) (D = denotes the centroid of C_5H_5).

spectra of **11a,b** and **12a,b** is that the phenyl carbon atoms close to the phosphorus nuclei show resonance signals with triplet and/or doublet-of-triplet multiplicities (Experimental Section). Metzinger has shown within a study of symmetric diphosphanes that triplet multiplicities for protons occur, when the *P,P* coupling constant J_{PP} exceeds the 10-fold value of J_{HP} ($J_{PP} \geq 10J_{HP}$), exposing such a signal pattern as deceptively simple.[58,59] Furthermore, due to the prochirality, two sets of signals were detected for the phenyl substituents at each phosphorus atom. The $^{31}P\{^1H\}$ NMR spectra of **11a,b** and **12a,b** display one resonance signal for the dppe ligands at 120 ppm for the iron complexes and at 100 ppm for the ruthenium

DOI: 10.1021/acs.organomet.5b00104
Organometallics XXXX, XXX, XXX−XXX

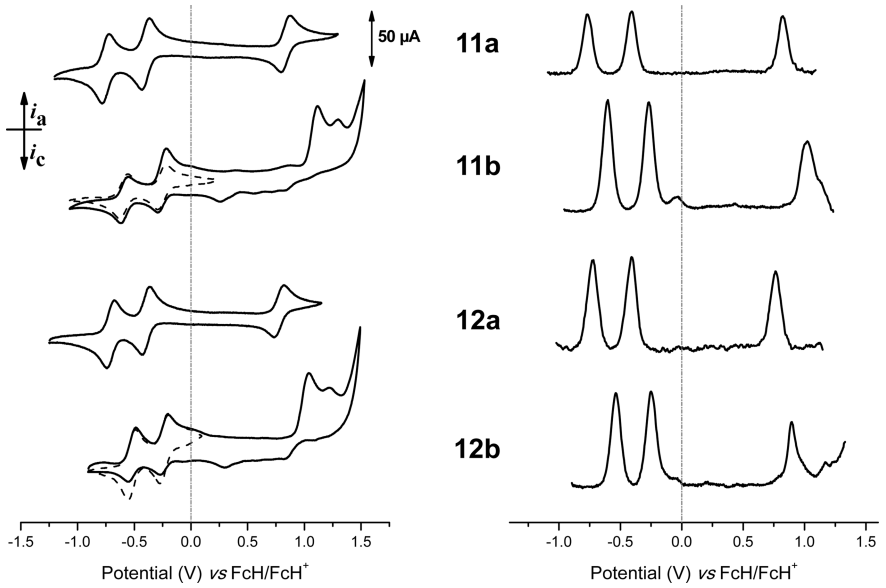

Figure 3. Voltammograms of dichloromethane solutions containing 1.0 mmol·L^{-1} of **11a,b** or **12a,b** at 25 °C. Supporting electrolyte [^{n}Bu$_4$N][B(C$_6$F$_5$)$_4$] (0.1 mol·L^{-1}). Left: Cyclic voltammograms (scan rate: 100 mV·s^{-1}). Right: Square-wave voltammograms (scan rate: 1 mV·s^{-1}). Dotted lines: CVs of **11b** and **12b** in a low potential range including only the redox events of the half-sandwich termini.

species (Experimental Section). A characteristic $\nu_{C\equiv C}$ vibration (**11a**, 2049 cm^{-1}; **11b**, 2062 cm^{-1}; **12a**, 2044 cm^{-1}; **12b**, 2053 cm^{-1}) is observed for the alkynyl unit in **11a,b** and **12a,b** in the IR spectra, which is in accordance with metal-coordinated acetylides.[13−15,55,56,60]

The molecular structures of **11a** (Figure 1) and **12a,b** (Figure 2) in the solid state were determined by single-crystal X-ray diffraction analysis. The respective organometallic compounds were crystallized by diffusion of hexane into a tetrahydrofuran solution containing **11a** or diffusion of toluene into a dichloromethane solution containing **12a** or **12b** at ambient temperature. Important bond distances (Å), bond angles (deg), and torsion angles (deg) are summarized in the captions of Figures 1 and 2. For crystal and structure refinement data see the Experimental Section.

Compounds **11a** and **12a,b** crystallize in the monoclinic space group $P2_1/c$ with one molecule in the asymmetric unit. Comparing the central five-membered heterocyclic cores, significant differences between the *C,C* single (C2−C3) and *C,C* double (C1−C2 and C3−C4) bonds[57,61] are present in **11a** and **12a** (C−C: **11a**, 1.413(4); **12a**, 1.411(5); longest C═C bond: **11a**, 1.363(4); **12a**, 1.359(5) Å) in contrast to **12b** (C−C: 1.387(5); longest C═C bond: 1.369(5) Å), which indicates a higher delocalization in the Ru-containing thiophene. To the best of our knowledge, the only reported and crystallographically characterized examples of *end-on* transition metal bonded MC≡C−^{c}C$_4$H$_2$E−C≡CM heterocyclic compounds contain Au, Pt, and Hg metal fragments (E = S), and the C≡C bond lengths are similar to the ones observed for **11a**, **12a**, and **12b**.[62−65] The M−M (M = Fe, Ru) distances in **11a** and **12a,b** increase, as expected, by increasing the size of the transition metal atoms (Fe: **11a**, 10.9056(5); **12a**, 11.3397(7); Ru: **12b**, 11.6880(5) Å) and, furthermore, by changing the heteroelement of the five-membered ring from oxygen (**11a**, 10.9056(5) Å) to sulfur (**12a**, 11.3397(7) Å).[45]

In **11a** and **12a,b** the size of the metal determines the M−centroid cyclopentadienyl distances (= D of C$_5$H$_5$) (average Fe−D: 1.72; average Ru−D: 1.90 Å), while the M−P distances (Fe−P: 2.1564(7) to 2.1721(7); Ru−P: 2.2472(10) to 2.2595(9) Å) are not that sensitive (Figures 1 and 2). The P−M−P angle decreases somewhat from M = Fe (**11a** and **12a**, 85.25(3)° to 85.83(3)°) to Ru (**12b**, 82.91(3)° and 83.28(4)°). The metallocenyl substituents slightly bend out of the heterocyclic plane, with the maximum reached for the metal ions (**11a**, 0.351(8); **12a**, 0.403(11); **12b**, 0.538(10) and −0.500(10) Å). This results in a somewhat C-shaped bending for **11a** and **12a** and an S-shape for **12b** (Figure SI1). The rotation of the C$_5$H$_5$ ring of the (η^5-C$_5$H$_5$)(P$_2$)MC≡C fragments (M = Fe, Ru; P$_2$ see Table SI1) toward each other reveals an *anti*-arrangement for **11a** and **12a,b**, which is in accordance with the only literature-reported example for M = Fe,[37] whereas for M = Ru also deviating conformations are reported (Table SI1).[36,37,66−73]

Electrochemistry. The electrochemical properties of **11a,b** and **12a,b** have been determined by cyclic voltammetry (CV) and square-wave voltammetry (SWV) (Figure 3) (dichloromethane solutions containing the respective analyte (1.0 mM) and [^{n}Bu$_4$N][B(C$_6$F$_5$)$_4$] (0.1 M) as supporting electrolyte).[46,74−80] The data of the CV measurements have been recorded at a scan rate of 100 mV·s^{-1} at 25 °C and are summarized in Table 1. All redox potentials are referenced to the FcH/FcH$^+$ redox couple ($E^{o\prime}$ = 0 mV, FcH = Fe(η^5-C$_5$H$_5$)$_2$).[81]

The metal atoms M (= Fe, Ru) of **11a,b** and **12a,b** could be oxidized separately, showing two reversible redox events (Figure 3, Table 1). In addition to the redox events of the half-sandwich moieties, a reversible redox process of the heterocyclic backbone was observed at higher potential, for **11a** at $E^\circ_3{}'$ = 835 mV and **12a** at $E^\circ_3{}'$ = 775 mV (Table 1). Compared to compounds **11a** and **12a** the redox events of the ruthenium derivatives **11b** and **12b** are shifted to anodic potentials (Table 1), indicating that the ruthenium metal center is more difficult to oxidize. This fact is supported by, for example, 9,10-((η^5-C$_5$Me$_5$)(dppe)MC≡C)$_2$-^{c}C$_{10}$H$_8$[17,32] (dichloromethane, [N(^{n}Bu)$_4$][PF$_6$] as supporting electrolyte; M = Fe, $E^\circ_1{}'$ = −400 mV; M = Ru, $E^\circ_1{}'$ = −170 mV) and 2,5-

DOI: 10.1021/acs.organomet.5b00104
Organometallics XXXX, XXX, XXX−XXX

Table 1. Cyclic Voltammetry Data (Potentials *vs* FcH/FcH$^+$) with a Scan Rate of 100 mV·s^{-1} at a Glassy Carbon Electrode of 1.0 mmol·L^{-1} Solutions of the Analytes in Anhydrous Dichloromethane Containing 0.1 mol·L^{-1} of [^{n}Bu$_4$N][B(C$_6$F$_5$)$_4$] as Supporting Electrolyte at 25 °C

compd	$E^\circ_1{}'$ (mV)[a] (ΔE_p (mV))[b]	$E^\circ_2{}'$ (mV)[a] (ΔE_p (mV))[b]	$E^\circ_3{}'$ (mV)[a] (ΔE_p (mV))[b]	$\Delta E^{\circ\prime}$ (mV)[c]	K_C[d]
11a	−750 (60)	−400 (66)	835 (84)	350	9.33 × 10^5
11b	−595 (72)	−255 (76)	1015[e]	340	5.20 × 10^5
12a	−710 (64)	−395 (65)	775 (83)	315	2.21 × 10^5
12b	−520 (64)	−235 (76)	895[e]	285	6.87 × 10^4

[a]$E^{\circ\prime}$ = formal potential. [b]ΔE_p = difference between oxidation and reduction potential. [c]$\Delta E^{\circ\prime}$ = potential difference between the two metal-based redox processes. [d]K_C = comproportionation constant (RT ln K_C = $\Delta E^{\circ\prime}F$). [e]Oxidation potential E_{pa}.

diferrocenyl/ruthenocenyl thiophene ($E^\circ_1{}'$ = −94 mV, dichloromethane, [N(^{n}Bu)$_4$][B(C$_6$F$_5$)$_4$];[77] $E^\circ_1{}'$ = 281 mV, dichloromethane, [N(^{n}Bu)$_4$][BF$_4$]),[82] which show a similar trend of the potential values in accordance with the different ionization potentials of Fe^{2+} and Ru^{2+}, respectively.[83] In the cyclic voltammogram of **11b** and **12b**, however, an irreversible oxidation for the heterocyclic core and further oxidation (**11b**, 1300 mV; **12b**, 1215 mV) and reduction processes (between 200 and 1000 mV) occur (Figure 3). As a consequence of these irreversible events, the follow-up products most likely decompose, and hence the concentration of **11b** and **12b** in solution is reduced. Therefore, measurements in which a higher reversal potential is applied showed a less reversible behavior for $E^\circ_1{}'$ and $E^\circ_2{}'$ of the half-sandwich moieties (Figure 3).

The redox splitting $\Delta E^{\circ\prime}$ between the MCp(dppe) moieties in **11a,b** and **12a,b** decreases from the furan (**11a**, 350 mV; **11b**, 340 mV) to the thiophene species (**12a**, 315 mV; **12b**, 285 mV) (Table 1). A further decreasing trend is found from the iron- (**11a**, **12a**) to the ruthenium-containing compounds (**11b**, **12b**). A comparison of **11a** and **12a** with 2,5-diferrocenyl heterocycles (furan, $\Delta E^{\circ\prime}$ = 290 mV; thiophene, $\Delta E^{\circ\prime}$ = 260 mV)[77] shows a similar decreasing trend of the redox separation. This progress can be explained with the stronger electronic coupling of the furan to the ferrocenyls or half-sandwich moieties, compared to thiophene, caused by the better overlap of the participating orbitals.[77] Furthermore, the stronger electron donor capabilities of the FeCp(dppe) moiety[84] as well as the direct metal−carbon bond are beneficial concerning electronic coupling to the heterocyclic bridge, when compared with the ferrocenyl analogues, and thus higher redox separations can be achieved. In contrast to the iron complexes, RuCp(dppe) termini are mixing more efficiently with the C≡C π-system, giving a higher ligand-based radical character of the frontier orbitals after oxidation,[7,85] which in turn leads to a destabilization of the aromatic bridging system. The observed redox separations are in the same range as the Cp*(dppe)-MC≡C-substituted thiophenes (M = Fe, $\Delta E^{\circ\prime}$ = 340 mV;[55] M = Ru, $\Delta E^{\circ\prime}$ = 320 mV),[56] furan (M = Fe, $\Delta E^{\circ\prime}$ = 440 mV),[86] and *N*-methyl pyrrole (M = Fe, $\Delta E^{\circ\prime}$ = 355 mV).[86] The high $\Delta E^{\circ\prime}$ values indicate intramolecular electronic interactions between the metal centers M (M = Fe, Ru) through the 2,5-bis(ethynyl)heterocyclic core. The large K_C values (Table 1) indicate sufficient thermodynamic stability of the mixed-valent species, and therefore, these molecules are well suited for spectroelectrochemical investigations (*vide infra*).

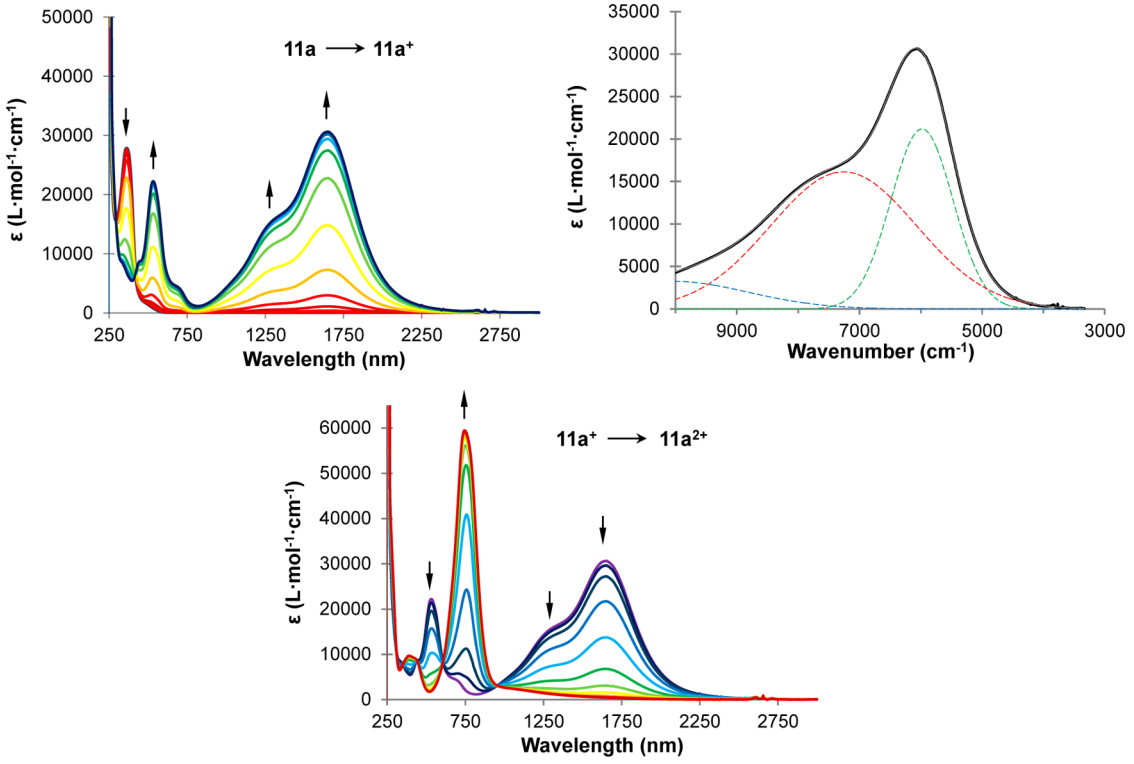

Figure 4. UV−vis/NIR spectra of **11a** at rising potentials vs Ag/AgCl: −200 to 250 mV (left top), 250 to 1000 mV (bottom). Right top: Deconvolution of the NIR absorptions at 250 mV of *in situ* generated **11a**$^+$ using three Gaussian-shaped graphs. Measurement conditions: 25 °C, dichloromethane, 0.1 mol·L^{-1} [^{n}Bu$_4$N][B(C$_6$F$_5$)$_4$] as supporting electrolyte.

DOI: 10.1021/acs.organomet.5b00104
Organometallics XXXX, XXX, XXX−XXX

Spectroelectrochemisry. *1. UV–vis/NIR and IR Spectroelectrochemistry.* The spectroelectrochemical UV–vis/NIR and IR measurements were performed in an OTTLE (optically transparent thin-layer electrochemistry) cell (quartz windows for UV/vis–NIR, CaF_2 windows for IR).[87] Dry dichloromethane solutions containing 0.1 mol·L^{-1} of [^{n}Bu$_4$N][B(C$_6$F$_5$)$_4$] as the supporting electrolyte and 2.0 mmol·L^{-1} of **11a,b** or **12a,b** were used at 25 °C. The potentials have been increased stepwisely using a step height of 25, 50, or 100 mV, whereby the neutral binuclear complexes **11a,b** and **12a,b** were oxidized to mixed-valent **11a,b**$^+$ and **12a,b**$^+$, resepectively, and finally to dicationic **11a,b**$^{2+}$ and **12a,b**$^{2+}$ (**11a**$^{n+}$, Figure 4; **11b**$^{n+}$, **12a,b**$^{n+}$ Supporting Information, Figures SI2–SI4; n = 0, 1, 2).

Neutral **11a,b** and **12a,b** showed ligand-centered $\pi \rightarrow \pi^*$ transitions[57] at 350 to 400 nm in the visible region of the spectrum, while, as expected, no absorptions could be detected in the NIR region (1000–3000 nm). Upon potential increase, intense absorptions between 1000 and 2000 nm were observed, demonstrating the formation of mixed-valent species **11a,b**$^+$ and **12a,b**$^+$. With further oxidation to dicationic **11a,b**$^{2+}$ and **12a,b**$^{2+}$ the absorptions disappear. Simultaneously, a new band at ca. 750 nm occurs, which can be assigned to an LMCT transition (ligand-to-metal charge transfer).[55,56] Deconvolution of the spectra of **11a,b**$^+$ and **12a,b**$^+$ was applied to determine the physical parameters (wavenumber (ν_{max}), extinction (ε_{max}), full-width at half-maximum (fwhm) ($\Delta\nu_{1/2}$)) of the excitations in the NIR region. The sum of the three overlapping Gaussian-shaped functions reflects the experimental graph. While the small and broad Gaussian function at around 10 000 cm^{-1} represents an LMCT transition (Table 2, Figures 4 and SI2–SI4), the band shape reveals two low-energy $\pi(d\pi) \rightarrow \pi^*(d\pi)$ transitions, involving the metal–ligand–metal setup.[88]

Table 2. UV–vis/NIR Data of 11a,b$^+$ and 12a,b$^+$[a]

compd	transition	ν_{max} (cm^{-1})	ε_{max} (L·mol^{-1}·cm^{-1})	$\Delta\nu_{1/2}$ (cm^{-1})
11a$^+$	$\pi(d\pi) \rightarrow \pi^*(d\pi)$	5980	21 190	1190
	$\pi(d\pi) \rightarrow \pi^*(d\pi)$	7260	16 135	2810
	LMCT	10 040	3250	2890
11b$^+$	$\pi(d\pi) \rightarrow \pi^*(d\pi)$	8200	7530	1170
	$\pi(d\pi) \rightarrow \pi^*(d\pi)$	9660	6250	2850
	LMCT	11 180	2550	5900
12a$^+$	$\pi(d\pi) \rightarrow \pi^*(d\pi)$	5515	17 900	1180
	$\pi(d\pi) \rightarrow \pi^*(d\pi)$	6770	16 460	3090
	LMCT	9500	2170	1860
12b$^+$	$\pi(d\pi) \rightarrow \pi^*(d\pi)$	7675	12 880	1580
	$\pi(d\pi) \rightarrow \pi^*(d\pi)$	9205	7460	1395
	LMCT	10 590	5550	2630

[a]In dichloromethane containing 0.1 mol·L^{-1} of [N^{n}Bu$_4$][B(C$_6$F$_5$)$_4$] as supporting electrolyte at 25 °C.

The band shapes fulfill the criteria for class III systems based on the two-state Hush model[89,90] for symmetric mixed-valent species, since the excitations are very intense ($\varepsilon_{max} \geq$ 5000 L·mol^{-1}·cm^{-1}). While the fwhm of the second excitation fits rather to a class II IVCT band, the small fwhm of the lower energy absorption complies with the class III criterion ($\Delta\nu_{1/2} \leq$ 2000 cm^{-1}) (Table 2).[91] The solvatochromic behavior of these absorptions was studied exemplary with **11b** using solvents with different dipole moments μ (dichloromethane (μ = 1.60 D), acetonitrile (μ = 3.93 D), propylene cabonate (μ = 4.90 D)).[92] The measurements proved solvent independency for both absorptions in the NIR range of the spectrum (Figure 5), indicating strong intramolecular electronic interactions between

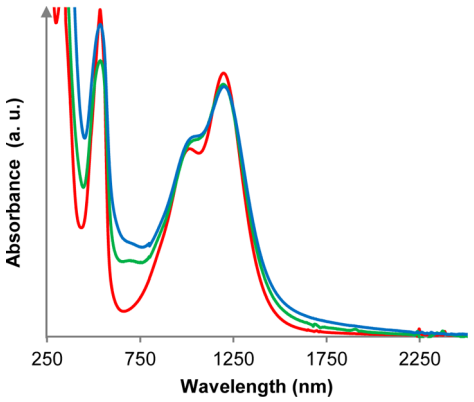

Figure 5. Solvent-dependency of **11b**$^+$ (2.0 mmol·L^{-1}) in dichloromethane (red), acetonitrile (blue), and propylene carbonate (green). Measurement conditions: 25 °C, 0.1 mol·L^{-1} [^{n}Bu$_4$N][B(C$_6$F$_5$)$_4$] as supporting electrolyte.

the metal centers M/M$^+$ (**11a** and **12a**, Fe(II)/Fe(III); **11b** and **12b**, Ru(II)/Ru(III)) through the bis(alkynyl) heterocyclic core. The MCp*(dppe)-substituted thiophene (M = Fe,[55] M = Ru[56]) and furan analogues (M = Fe)[86] show absorptions similar to the NIR bands of **11a** and **12a,b**. Different ancillary ligands (Cp*), solvent effects, and applied electrolytes are responsible for a variation of the intensity and band shape. Nevertheless, Lapinte[55] and Liu[56] found solvent-independent excitations with a high-energy shoulder, revealing two superimposed transitions by deconvolution.

A possible reason for the complex excitation phenomena in the NIR region of mixed-valent **11a,b**$^+$ and **12a,b**$^+$ is presumably related to the presence of a couple of thermally accessible conformers with varying excitation energies (Figure 6). Kaupp and Low demonstrated this behavior on the

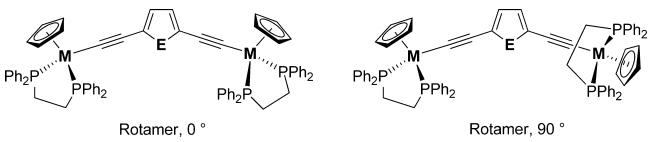

Figure 6. Different conformations of the half-sandwich unit in **11** and **12** with respect to the bis(alkynyl) heterocyclic plane.

examples of [{Ru(dppe)Cp*}$_2$(μ-C≡CC$_6$H$_4$C≡C)]$^+$ and [*trans*-{Ru(dppe)$_2$Cl}$_2$(μ-C≡CC$_6$H$_4$C≡C)]$^+$.[93] The latter complex is less likely to form rotational conformers, due to its more symmetric coordination sphere, but [{Ru(dppe)Cp*}$_2$(μ-C≡CC$_6$H$_4$C≡C)]$^+$ can build conformers in which the orbitals of the redox-active unit are overlapping with different orbitals of the bridging units' π-system. Time-dependent DFT calculations showed that conformers with a lower P–Ru–Ru–P dihedral angle showed a more delocalized electronic situation.[93]

The electronic coupling parameter H_{ab},[89−91] which indicates the strength of the electronic interaction between two redox-active termini, has been calculated according to the equation H_{ab} = 1/2 ν_{max} and is between 2750 and 4830 cm^{-1} for **11a,b** and **12a,b** (2,5-(Cp*(dppe)FeC≡C)$_2$-^{c}C$_4$H$_2$O: H_{ab} = 2665 cm^{-1};[86] 2,5-(Cp*(dppe)FeC≡C)$_2$-^{c}C$_4$H$_2$S: H_{ab} = 2515 cm^{-1};[55] 2,5-(Cp*(dppe)RuC≡C)$_2$-^{c}C$_4$H$_2$S: H_{ab} = 3523

DOI: 10.1021/acs.organomet.5b00104
Organometallics XXXX, XXX, XXX–XXX

cm^{-1}).[56] The coupling parameters of **11a,b** and **12a,b** are in a comparable range, for example, the Creutz–Taube ion (H_{ab} = 3205 cm^{-1}).[94] Calculation of the Γ parameter ($\Gamma = 1 - (\Delta\nu_{1/2}/(\Delta\nu_{1/2})_{theo})$)[91] of mixed-valent **11a,b**$^+$ and **12a,b**$^+$, a classification criterion of Brunschwig et al.[95] for mixed-valent compounds, gives values of 0.22 and 0.73 for the two NIR excitations (Tables 2 and 3). With Γ values ≥ 0.5 a further indication for strongly coupled systems is given. However, Γ values ≤ 0.5 of the second $\pi(d\pi) \rightarrow \pi^*(d\pi)$ transitions rather classify **11a,b**$^+$ and **12a,b**$^+$ as class II species.[95] The deconvolution methodology described above utilizes Gaussian-shaped functions to simulate the experimental spectra. Part of the reason for the small bandwidths within class III systems is a low-energy cutoff of the bands at ν_{max},[88] and thus a Gaussian-shaped spectral simulation overestimates the bands' slope at the high-energy side. Since the second NIR absorption overlaps with the high-energy side of the main absorption, the parameters derived from this band should be handled with care. In this respect the high-energy NIR transition for all compounds cannot be assigned to class II or III unambiguously. While this band showed solvent-independence, a typical class III feature, the physical parameters derived from deconvolution (especially the fwhm value and the Γ criterion), however, argue for a class II assignment.

Table 3. H_{ab} and Γ Parameters of 11a,b$^+$ and 12a,b$^+$ for the $\pi(d\pi) \rightarrow \pi^*(d\pi)$ Transition

compd	transition	H_{ab} (cm^{-1})[a]	$\Delta\nu_{1/2(theo)}$ (cm^{-1})	Γ[d]
11a$^+$	$\pi(d\pi) \rightarrow \pi^*(d\pi)$	2990	2628	0.55
	$\pi(d\pi) \rightarrow \pi^*(d\pi)$/IVCT	3630/1083[b]	4095	0.31
11b$^+$	$\pi(d\pi) \rightarrow \pi^*(d\pi)$	4100	4352	0.73
	$\pi(d\pi) \rightarrow \pi^*(d\pi)$/IVCT	4830/760[b,c]	4724	0.39
12a$^+$	$\pi(d\pi) \rightarrow \pi^*(d\pi)$	2758	3569	0.67
	$\pi(d\pi) \rightarrow \pi^*(d\pi)$/IVCT	3385/1065[b]	16460	0.22
12b$^+$	$\pi(d\pi) \rightarrow \pi^*(d\pi)$	3838	4210	0.63
	$\pi(d\pi) \rightarrow \pi^*(d\pi)$/IVCT	4603/545[b]	4611	0.69

[a]Calculated with the equation $H_{ab} = {}^1/_2\nu_{max}$. [b]Calculated with the equation $H_{ab} = 2.06 \times 10^{-2} \times ((\nu_{max}\varepsilon_{max}\Delta\nu_{1/2})^{1/2}/r_{ab})$. As r_{ab} geometrical metal–metal distances derived from X-ray crystallographic data were used, see X-ray crystallography part. [c]r_{ab} (11.25 Å) has been estimated from the other values for **11a**$^+$ and **12a,b**$^+$. [d]Calculated with the equation $\Gamma = 1 - (\Delta\nu_{1/2}/(\Delta\nu_{1/2})_{theo})$.

The electronic coupling for the furan derivatives **11a,b** is higher than that of isostructural thiophenes **12a,b** (Table 3, Figure 7). This difference most probably causes the individual differences in the respective $\Delta E^{\circ\prime}$ values as contribution to the resonance stabilization (**11a**, $\Delta E^{\circ\prime}$ = 350 mV, H_{ab} = 2990/3630 cm^{-1} → **12a**, $\Delta E^{\circ\prime}$ = 315 mV, H_{ab} = 2758/3385 cm^{-1}; **11b**, $\Delta E^{\circ\prime}$ = 340 mV, H_{ab} = 4100/4830 cm^{-1} → **12b**, $\Delta E^{\circ\prime}$ = 285 mV, H_{ab} = 3838/4603 cm^{-1}). The resonance stabilization term (ΔG_r), as a contribution to the free energy of comproportionation, can be calculated for class III systems according to eq 1, whereas λ is the diadiabatic reorganization energy.[91,95,96]

$$\Delta G_r = -2(H_{ab} - \lambda/4) \quad (1)$$

It is reasonable that varying the heterocyclic unit (**11** → **12**) has no significant effect on the value of λ. Therefore, changes in ΔG_r are predominantly caused by changes in the coupling parameter H_{ab}. However, changing the metal from iron to ruthenium (**a** → **b**) has a significant impact on the diadiabatic reorganization energy, and thus not only do the different coupling parameters contribute to ΔG_r and consequently to $\Delta E^{\circ\prime}$, but also the influence of λ becomes noticeable. As a result of this, the ruthenium-containing molecules **11b** and **12b** showed smaller $\Delta E^{\circ\prime}$ values despite possessing higher coupling parameters H_{ab}. It can be concluded that the diadiabatic reorganization energy λ for the softer ruthenium atom, compared to iron, is smaller and therefore overcompensates H_{ab}.

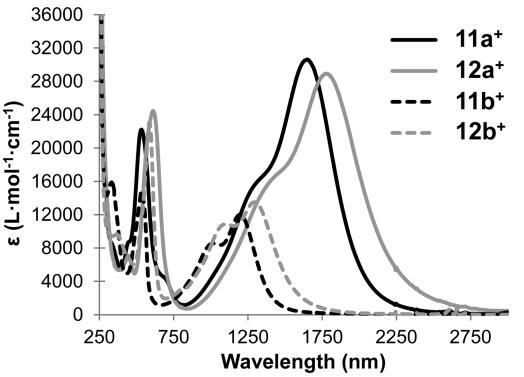

Figure 7. Comparison of the UV–vis/NIR spectra of **11a**$^+$,**b**$^+$ and **12a**$^+$,**b**$^+$. Measurement conditions: 2.0 mM analyte, 25 °C, dichloromethane, 0.1 mol·L^{-1} [^{n}Bu$_4$N][B(C$_6$F$_5$)$_4$] as supporting electrolyte.

The IR-active alkynyl unit enables us to investigate the degree of charge delocalization of the mixed-valent species on the IR time scale.[97,98] During the *in situ* IR spectroelectrochemical measurements the characteristic $\nu_{C\equiv C}$ vibrations at ca. 2050 cm^{-1} for the neutral complexes **11** and **12**, respectively, disappear (Figures 8 and SI5–SI7). Simultaneously a new band at lower energy (1980–1960 cm^{-1}) appears owing to the formation of a mixed-valent species and therefore to a partially cumulenic character of the original (η^5-C_5H_5)(dppe)MC≡C unit (Figures 8 and SI5–SI7, Table 4). The detection of one narrow stretching vibration for **11a,b**$^+$ and **12a,b**$^+$ indicates that the single electron is delocalized between the two metal centers. Hence, complexes **11a,b** and **12a,b** are strongly coupled systems on the IR time scale. In comparison, for compounds with similar structural motifs, the appearance of two distinctive $\nu_{C\equiv C}$ stretching vibrations is observed within class II systems.[19,35,36] Upon close inspection of the IR characteristics of **11a,b**$^+$ and **12a,b**$^+$ small shoulders at ca. 1945 cm^{-1} can be found, which may indicate the presence of a thermally accessible conformer with a more localized electronic structure. Further oxidation to dicationic **11a,b**$^{2+}$ and **12a,b**$^{2+}$ and the increase of the cumulenic character of the vibration led to a formal hypsochromical shift of the absorption band to 1920 cm^{-1}.

To support the interpretations of the UV–vis/NIR and ESR spectra, exemplarily mononuclear complex 2-(RuCp(dppe)-C≡C)-thiophene (**15**) was synthesized. The cyclic voltammogram of **15** showed only one irreversible oxidation process of the Ru(dppe)Cp group at E_{pa} = −170 mV (see Supporting Information, Figure SI8). It is suspected that upon oxidation a reactive radical cation is formed and polymerization as well as other side reactions can occur through the unsubstituted 5 position. Therefore, further spectroelectrochemical investigations were excluded. To suppress such processes, 2-(RuCp-(dppe)-C≡C)-5-methyl thiophene (**16**) was synthesized. However, the CV also showed an irreversible oxidation at E_{pa}

DOI: 10.1021/acs.organomet.5b00104
Organometallics XXXX, XXX, XXX–XXX

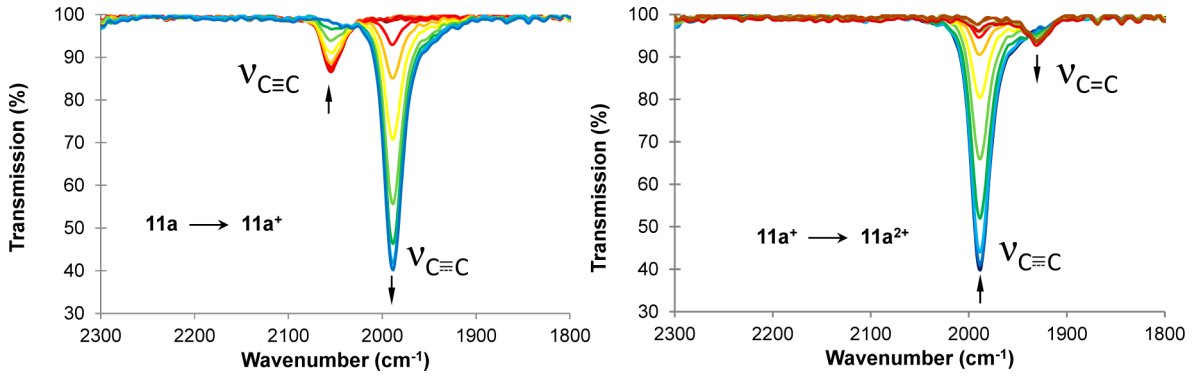

Figure 8. IR spectroelectrochemical spectra of **11a** at rising potentials vs Ag/AgCl. Left: −200 mV to 510 mV (**11a** → **11a**$^+$). Right: 510 mV to 1000 mV (**11a**$^+$ → **11a**$^{2+}$). The blue line belongs to the mixed-valent species **11a**$^+$ and is labeled with $\nu_{C\equiv C}$. Measurement conditions: 25 °C, dichloromethane solution containing 10.0 mmol·L^{-1} of **11a**, 0.1 mol·L^{-1} of [N^{n}Bu$_4$][B(C$_6$F$_5$)$_4$] as supporting electrolyte.

Table 4. Spectroelectrochemical IR Data for 11a,b^{n+} and 12a,b^{n+} (n = 0, 1, 2)

compd	$\nu_{C,C}$ (cm^{-1}) (n = 0)	$\nu_{C,C}$ (cm^{-1}) (n = 1)	$\nu_{C,C}$ (cm^{-1}) (n = 2)
11a^{n+}	2052	1986	1930
11b^{n+}	2065	1973	1932
12a^{n+}	2048	1982	1919
12b^{n+}	2058	1961	1921

= −190 mV (Supporting Information, Figure SI8). Additionally, on increasing the potential range to 900 mV a second more quasi-reversible redox event (E_{pa} = 600 mV) was observed, which can be assigned to the oxidation of the thiophene core. In contrast to the electrochemically stable benzene-Ru(dppe)-Cp from Low,[99] the thiophenes are susceptible to diverse side reactions when oxidized.

2. ESR Spectroelectrochemistry. Further confirmation of the delocalized nature of the radical cations **11a,b**$^+$ and **12a,b**$^+$ was obtained by *in situ* ESR spectroelectrochemistry studies and DFT calculations. Figure 9 shows the X-band ESR spectra measured *in situ* during electrochemical oxidation of the compounds at their first oxidation potentials. All species readily formed ESR-detectable signals at corresponding potentials

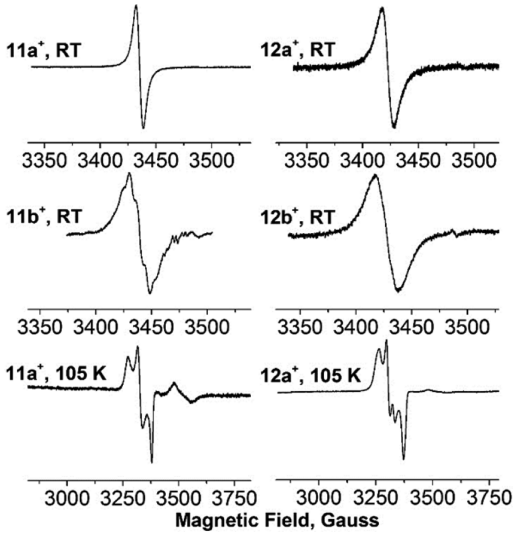

Figure 9. ESR spectra of electrochemically generated cation radicals measured at room temperature (RT) and in frozen solution (105 K). Note the change of the sweep width for the frozen solutions.

whose intensity evolution during the electrochemical cycles correlated well with the transferred charge. The spectra of **11a**$^+$, **12a**$^+$, and **12b**$^+$ are featureless lines with the effective peak width of 6, 11, and 22 G, respectively. For **11b**$^+$ a hyperfine structure is characteristic (albeit not fully resolved), the origin of which is discussed below.[100] The isotropic g-factor values for all radical-cations are close to 2.03−2.04 (Table 5); broad-field

Table 5. Experimental and DFT-Computed Calculated g Values for 11a,b$^+$ and 12a,b$^+$

compd		g_1	g_2	g_3	Δg	g_{iso}[a]
11a$^+$	expt	1.9997	2.0316	2.0650	0.0653	2.0347
	calcd (0,0)	2.0007	2.0284	2.0331	0.0324	2.0207
	calcd (0,90)	2.0067	2.0366	2.1283	0.1216	2.0572
12a$^+$	exp.	2.0058	2.0463	2.0728	0.0670	2.0423
	calcd (0,0)	2.0017	2.0345	2.0437	0.0421	2.0266
	calcd (0,90)	2.0072	2.0395	2.1409	0.1337	2.0626
11b$^+$	expt	n/a	n/a	n/a	n/a	2.0322
	calcd (0,0)	1.9991	2.0331	2.0522	0.0531	2.0281
	calcd (0,90)	1.9999	2.0235	2.0569	0.0570	2.0268
12b$^+$	expt	n/a	n/a	n/a	n/a	2.0389
	calcd (0,0)	1.9992	2.0396	2.0603	0.0610	2.0330
	calcd (0,90)	2.0003	2.0286	2.0708	0.0704	2.0332

[a]Experimental g_{iso} values are for the room-temperature spectra; g_{iso} values obtained by averaging g-tensor components determined in frozen solution are 2.0321 for **11a**$^+$ and 2.0416 for **12a**$^+$.

scans did not reveal the presence of any other ESR signals. The g-factors are noticeably higher than the free electron value (2.0032) and point to a significant metal contribution to the spin density. At the same time, deviations from the free electron value can be considered as relatively small, when compared to Fe- and Ru-based radicals with predominant localization of the spin density on the metal centers.

Freezing solutions of **11a**$^+$ and **12a**$^+$ after their electrolysis afforded powder-like ESR spectra with rhombic symmetry. The experimentally determined diagonal elements of the g-tensor span the range from 1.9997 to 2.0321 in **11a**$^+$ and from 2.0058 to 2.0728 in **12a**$^+$. Anisotropy of the g-tensor, Δg, calculated as the difference between the largest and the smallest diagonal elements, is 0.0653 in **11a**$^+$ and 0.0670 in **12a**$^+$. Dong and Hendrickson[101] showed that anisotropy of the g-factor in radicals of mixed-valence complexes correlates with the electron transfer rate. In particular, the Δg values are smaller than 1.1 due to the delocalized spin density character. The values

DOI: 10.1021/acs.organomet.5b00104
Organometallics XXXX, XXX, XXX−XXX

determined in this work are much smaller than this threshold criterion, and thus the ESR study also confirms the delocalized nature of the complexes.

DFT Calculations. The electronic structures of **11a**,**b** and **12a**,**b** in the neutral and cationic states were studied by DFT calculations. First, atomic coordinates were optimized at the PBE/TZ2P level. Then, the frontier MO analysis, spin density distribution, time-dependent DFT calculations, and calculations of the ESR parameters were performed using a modified version of the B1LYP functional (denoted hereafter as B(35)LYP) in which the fraction of exact exchange was increased to 35% following the work of Kaupp et al.[93,102] They showed that this functional provides a balanced description of localization/delocalization phenomena in mixed-valence complexes. In the B(35)LYP calculations, also ZORA scalar-relativistic corrections and COSMO solvation corrections (dichloromethane, ε = 9.08) were considered. The basis set was a SARC-modified version of the def2-TZVP basis set specially tailored for calculations with ZORA correction (see the Supporting Information for further details of calculations).

Figure 10a shows the HOMO and HOMO−1 isosurfaces of **11a**, which are well representative also for the other complexes.

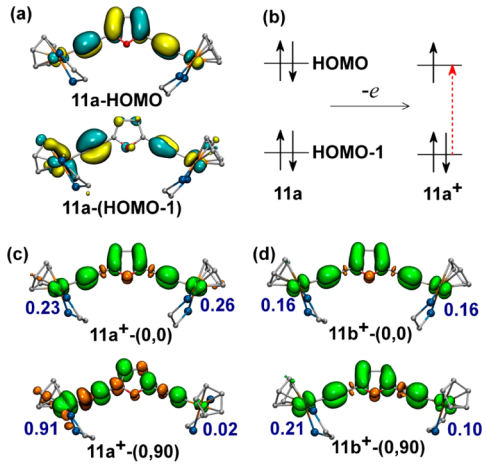

Figure 10. (a) HOMO and HOMO−1 in **11a**; (b) schematic description of the changes in MO population induced by oxidation and appearance of the new optical excitation (denoted by red arrow); (c) spin density isosurfaces in two rotamers of **11a**$^+$; (d) spin density isosurfaces in two rotamers of **11b**$^+$. In MO isosurfaces, yellow is "+" and cyan is "−"; in the spin density isosurface, green is "+" and orange is "−". Phenyl groups and hydrogen atoms are not shown for clarity.

The HOMO is delocalized over the bridging unit with a large contribution of the central heterocycle. Metal contributions are rather small but not negligible either. On the contrary, in the HOMO−1 the metal contribution is enhanced, whereas the heterocycle contribution is almost negligible. A large part of the HOMO−1 is also delocalized over the acetylide fragments. The relatively large gap between the two orbitals indicates delocalization of the cation radical. When compound **11a** is oxidized, the HOMO is depopulated and a new optical excitation appears as shown in Figure 10b, which is responsible for NIR bands in the absorption spectra of the cations.

Since rotation of the half-sandwich units may result in a significant variation of the electronic structure of the complexes and even change a delocalized system into a localized one, special attention was devoted to this point in the cationic structures. To define a rotamer, we used two numbers in parentheses, which correspond to rotation angles of each half-sandwich unit with respect to the heterocycle plane. In this notation, the rotamer shown in Figure 6, left, is described as (0,0), whereas the rotamer shown in Figure 6, right, with one unit rotated by 90° is denoted as (0,90). The studies of the potential energy surface at the PBE/TZ2P level showed that the structures with (0,0), (0,180), and (180,180) are almost isoenergetic and correspond to the energy minima, whereas the structures with the rotation angles of 90° are energy maxima (see Supporting Information for further details). At the B(35)LYP level, the rotamers (0,90) are only a few kJ·mol^{-1} less stable than rotamers (0,0). Relative energies of (0,90) rotamers of **11a**$^+$ and **12a**$^+$ with respect to (0,0) rotamers are only 4 and 1 kJ/·mol^{-1}, respectively. For **11b**$^+$ and **12b**$^+$ the energies of the (0,90) rotamers are somewhat higher, 11 and 10 kJ·mol^{-1}, respectively, but still remain rather small. Thus, free rotation of the half-sandwich units is expected at room temperature, and therefore the spectral characteristics measured experimentally are averaged responses of many rotamers.

Despite the similar energies, electronic structures of the rotamers can be substantially different. Figure 10c,d shows spin density distributions in (0,0) and (0,90) rotamers of **11a**$^+$ and **11b**$^+$ (similar surfaces are obtained for **12a**$^+$ and **12b**$^+$). In the (0,0) rotamers the spin density is equally distributed over the metal centers and the bridge (Figure 10) and the shape of the lobes roughly resembles that of the HOMO. Mulliken spin populations of the metal atoms are 0.23/0.26 in **11a**$^+$ and 0.16/0.16 in **11b**$^+$. The rotation of a half-sandwich unit by 90° results in significant changes of the spin density distribution, especially in **11a**$^+$. Spin populations of the metal atoms in the units at 0° are increased to 0.91 and 0.21 in **11a**$^+$ and **11b**$^+$, respectively, whereas those of the metal atoms in the rotated units are decreased to 0.02 in **11a**$^+$ and 0.10 in **11b**$^+$ (note that **11a**$^+$ and **12a**$^+$ suffer from rather large spin contaminations, and hence the values are probably too high). Thus, whereas (0,0) conformers are typical delocalized systems, (0,90) conformers exhibit a substantial degree of localization.

Coexistence of rotamers with localized and delocalized spin density distribution may be the reason for the two-band absorption pattern in the NIR range (Figures 4, 5, 7, and Supporting Information Figures SI2−SI4) as proposed earlier by Kaupp, Low, and co-workers.[93] Indeed, TD-DFT computations show that the intense NIR excitation in (0,0) rotamers has lower energy than in (0,90) rotamers (Figure 11; note that TD-DFT systematically overestimates excitation energies). In Figure 11 also the difference electronic densities for the excitations with the highest oscillator strength are shown. Similar to the spin density distribution described in Figure 10, the different excitation density in (0,0) rotamers is equally delocalized over the two metals, whereas in (0,90) rotamers one of the metals has a higher contribution.

Variation of the spin density distribution with rotation of the half-sandwich entities also manifests itself in the EPR parameters, especially in the *g*-tensor diagonal elements and isotropic *g* value. Table 5 compares experimental values to the computed ones. Neither (0,0) nor (0,90) rotamers alone are able to describe the experimental data for **11a**$^+$ and **12a**$^+$. The DFT-predicted *g*-tensor anisotropy and the isotropic *g*-factor are too small in (0,0) rotamers and too large in (0,90) ones; however, their combination gives a reasonable match to the measured values.

Rotational flexibility significantly affects hyperfine coupling (hfc) constants. Average ^{31}P hfc constants in **11a**$^+$-(0,0) are 6.9

DOI: 10.1021/acs.organomet.5b00104
Organometallics XXXX, XXX, XXX−XXX

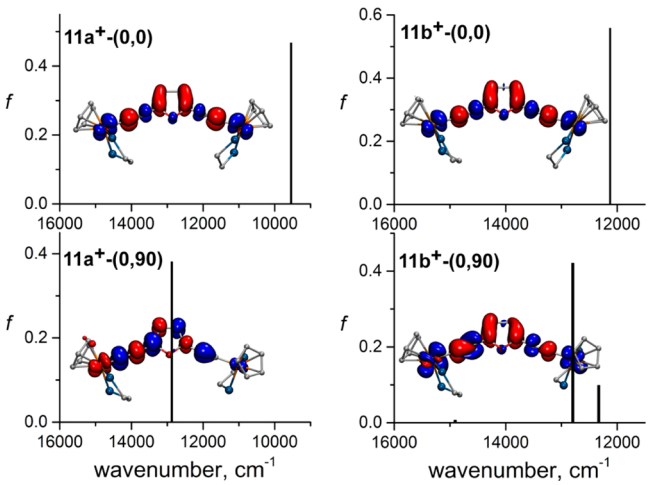

Figure 11. TD-DFT-predicted excitation spectra of **11a**$^+$ and **11b**$^+$ rotamers in the NIR range and difference densities for the most intense excitations (red is "+" and blue is "−"). Phenyl groups and hydrogen atoms are not shown for clarity.

G, and those of two ^{1}H nuclei in the heterocycle are −2.2 G. Preferential localization of the spin density near a half-sandwich unit in the (0,90) rotamer leads to a large asymmetry of hfc values: phosphorus atoms are now divided into two pairs with ^{31}P hfc constants of −10.7 and 1.2 G. ^{1}H constants in **11a**$^+$-(0,90) are 0.4 and −1.6 G. A similar situation is predicted for the rotamers of **12a**$^+$: ^{31}P hfc constants are 5.4 G in (0,0) and −12.1/1.1 G in the (0,90) rotamers, whereas ^{1}H values are −1.7 and −0.5 G. Thus, ^{31}P values in **11a**$^+$ and **12a**$^+$ have similar absolute values but an opposite sign in (0,0) and (0,90) rotamers and therefore upon thermal averaging compensate each other.

A less profound effect has the internal rotation on the hfc constants in **11b**$^+$ and **12b**$^+$. Here the ^{31}P hfc constants are near 10 G in (0,0) and 10.9/2.6 G in (0,90) rotamers, and hence thermal averaging is expected to produce values near 7−8 G. ^{1}H hfc constants are close to −2 G in both compounds. For the two isotopes of Ru with the nuclear spin 5/2 (^{99}Ru (12.7%), ^{101}Ru (17.1%)) theory predicts hfc values of about 6 G (see the Supporting Information for full details). Thus, in contrast to **11a**$^+$ and **12a**$^+$, **11b**$^+$ and **12b**$^+$ are predicted to have relatively large ^{31}P hfc constants and also non-negligible hyperfine coupling with the two Ru isotopes. This explains why the EPR signals of **11b**$^+$ and **12b**$^+$ are significantly broader at room temperature than their analogues **11a**$^+$ and **12a**$^+$. The hyperfine structure partially resolved in the radical cation of **11b**$^+$ can be assigned predominantly to the ^{31}P nuclei.

CONCLUSION

Within this study the synthesis of a series of iron and ruthenium half-sandwich alkynyl complexes bearing a thiophene or furan π-conjugated connectivity (2,5-((η^5-C_5H_5)(dppe)MC≡C)$_2$-^{c}C$_4$H$_2$E (E = O (**11**), S (**12**); M = Fe (**a**), Ru (**b**)) is reported. The appropriate Me_3SiC≡C-protected heterocycles were synthesized in a Sonogashira *C,C* cross-coupling reaction, and the following attachment of the MCp(dppe) moieties was realized in a three-step consecutive "one-pot" reaction. The influence of Fe and Ru and the heterocyclic core on the intramolecular electronic metal−metal interactions in the mixed-valent species has been investigated. The structures of **11a** and **12a,b** in the solid state were determined using single-crystal X-ray diffraction analysis showing *anti*-arrangements of the metal half-sandwich moieties toward each other. The electronic properties of **11a,b** and **12a,b** have been studied by electrochemical measurements, whereby the respective compounds show well-separated reversible one-electron redox events for the two redox-active termini. The calculated large K_C values (6.87×10^4 to 9.33×10^5) validate their high thermodynamic stability. Further spectroelectrochemical studies indicated that the thiophene and furan units as bridging ligands in **11a,b** and **12a,b**, respectively, are beneficial for intramolecular electron transfer studies in the mixed-valent species. Mixed-valent **11a,b**$^+$ and **12a,b**$^+$ reveal charge delocalization within the UV−vis/NIR and ESR and on the IR time scale. In UV−vis/NIR studies **11a,b**$^+$ and **12a,b**$^+$ show intense, narrow, and solvent-independent $\pi(d\pi) \rightarrow \pi^*(d\pi)$ absorptions. Due to the presence of a couple of thermally accessible conformers with varying excitation energies, two NIR absorptions are observed. The IR spectra give one narrow bathochromic shifted $\nu_{C\equiv C}$ stretching vibration for **11a,b**$^+$ and **12a,b**$^+$, due to the increasing cumulenic character of the (η^5-C_5H_5)(dppe)M═C═C moiety. For all compounds, the formation of cation radicals at the first reduction step was detected by ESR spectroscopy. The low anisotropy of the *g*-factor in frozen solution is in accordance with the delocalized nature of the species. These results characterize **11a,b** and **12a,b** as strongly coupled compounds according to the classification of Robin and Day[54] and enlarge the family of organometallic class III systems.[88,103,104] However, both spectroscopic (NIR, IR, ESR) and computational (DFT/TD-DFT) results are best described by a mixture of least two thermally accessible rotation conformers of the organometallic termini of **11a,b** and **12a,b**. While for one of the conformers (0,0) a delocalized structure is found, rotation of one of the redox-active moieties of 90° (0,90) results in a more localized behavior.

EXPERIMENTAL SECTION

General Conditions. All reactions were carried out under an atmosphere of argon using standard Schlenk techniques. Drying of hexane, diethyl ether, and dichloromethane was performed with a double column solvent filtration system, working pressure 0.5 bar. Tetrahydrofuran was purified by distillation from sodium/benzophenone ketyl, and methanol was purified by distillation from magnesium. Diisopropylamine was purified by distillation from calcium hydride.

Reagents. 2,5-Dibromothiophene (**4**), furan, KO^{t}Bu, *N*-bromosuccinimide, trimethylsilyl acetylene, copper(I) iodide, potassium carbonate, tetra-*n*-butylammonium fluoride, and ammonium hexafluorophosphate were purchased from commercial suppliers and used without further purification. 2,5-Dibromofuran,[76] 2,5-bis(trimethylsilyl)thiophene (**6**),[56] [Fe(η^5-C_5H_5)(η^2-dppe)Cl] (**7**),[22,105] [Ru(η^5-C_5H_5)(η^2-dppe)Cl] (**8**),[106] [Os(η^5-C_5H_5)(η^2-dppe)Br],[107] [^{n}Bu$_4$N][B(C_6F_5)$_4$],[47,75,76,79,80,108−111] and [PdCl$_2$(PPh$_3$)$_2$][112] were prepared according to published procedures.

Instruments. ^{1}H NMR (500.3 MHz), ^{13}C{^{1}H} NMR (125.8 MHz), and ^{31}P{^{1}H} NMR (202.5 MHz) spectra were recorded at 298 K in the Fourier transform mode. Chemical shifts are reported in δ units (parts per million) using undeuterated solvent residues as internal standard ($CDCl_3$: ^{1}H at 7.26 ppm and ^{13}C{^{1}H} at 77.16 ppm; C_6D_6: ^{1}H at 7.16 ppm and ^{13}C{^{1}H} at 128.06 ppm).

Single-Crystal X-ray Diffraction Analysis. Data for **11a** and **12a,b** were collected with a diffractometer using graphite-monochromatized Mo Kα (λ = 0.71073 Å) (**12a** and **12b**) or Cu Kα radiation (1.54184 Å) (**11a**). The molecular structures were solved by direct methods using SHELXS-97[113] and refined by full-matrix least-squares procedures on F^2 using SHELXL-97.[114] All non-hydrogen

DOI: 10.1021/acs.organomet.5b00104
Organometallics XXXX, XXX, XXX−XXX

atoms were refined anisotropically, and a riding model was employed in the treatment of the hydrogen atom positions. Graphics of the molecular structures have been created by using ORTEP.[115]

Electrochemistry. Measurements on 1.0 mmol·L^{-1} solutions of the analytes in anhydrous air-free dichloromethane containing 0.1 mol·L^{-1} of [^{n}Bu$_4$N][B(C$_6$F$_5$)$_4$] as supporting electrolyte were conducted under a blanket of purified argon at 25 °C. A three-electrode cell, which includes a Pt auxiliary electrode, a glassy carbon working electrode (surface area 0.031 cm^2), and a Ag/Ag$^+$ (0.01 mol·L^{-1} AgNO$_3$) reference electrode mounted on a Luggin capillary, was used. The working electrode was pretreated by polishing on a microcloth first with a 1 μm and then with a 1/4 μm diamond paste. The reference electrode was built from a silver wire inserted into a solution of 0.01 mol·L^{-1} [AgNO$_3$] and 0.1 mol·L^{-1} [^{n}Bu$_4$N][B(C$_6$F$_5$)$_4$] in acetonitrile in a Luggin capillary with a Vycor tip. This Luggin capillary was inserted into a second Luggin capillary with a Vycor tip filled with a 0.1 mol·L^{-1} dichloromethane solution of [^{n}Bu$_4$N][B(C$_6$F$_5$)$_4$].[47,75,76,78−80,109−111] Successive experiments under the same experimental conditions showed that all formal reduction and oxidation potentials were reproducible within ±5 mV. Experimentally potentials were referenced against an Ag/Ag$^+$ reference electrode, but results are presented referenced against ferrocene[116,117] (FcH/FcH$^+$ couple = 220 mV vs Ag/Ag$^+$, ΔE_p = 61 mV; FcH = Fe(η^5-C$_5$H$_5$)$_2$) as an internal standard as required by IUPAC.[81] When decamethylferrocene (Fc* = Fe(η^5-C$_5$Me$_5$)$_2$) was used as an internal standard, the experimentally measured potential was converted into E vs FcH/FcH$^+$ (under our conditions the Fc*/Fc*$^+$ couple was at −614 mV vs FcH/FcH$^+$, ΔE_p = 60 mV).[118] Data were then manipulated on a Microsoft Excel worksheet to set the formal redox potentials of the FcH/FcH$^+$ couple to $E^{\circ\prime}$ = 0.00 V. The cyclic voltammograms were taken after two typical scans and are considered to be steady-state cyclic voltammograms in which the signal pattern does not differ from the initial sweep.

IR and UV−vis/NIR Spectroelectrochemistry. The spectroelectrochemical measurements of **11a,b** and **12a,b** (2.0 mM) in anhydrous dichloromethane containing [^{n}Bu$_4$N][B(C$_6$F$_5$)$_4$] (0.1 M) as the supporting electrolyte were performed in an OTTLE cell with quartz (UV/vis−NIR) or CaF$_2$ windows (IR)[87] at 25 °C. Between the spectroscopic measurements the applied potentials have been increased stepwisely using a step height of 25, 50, or 100 mV. At the end of the measurements the analyte was reduced at −500 mV for 15 min, and an additional spectrum was recorded to prove the reversibility of the oxidations.

ESR Spectroelectrochemical Measurements. For the electrochemical ESR investigations a special flat cell[119−121] (dimensions 0.5 × 8 × 40 mm^3) with quartz windows was used. The three-electrode cell utilized a laminated platinum sheet as a working electrode (diameter of the opening in the lamination foil 4 mm) and a platinum wire as reference and counter electrode. The measurements were carried out on 1.0 mmol·L^{-1} solutions of the analytes in anhydrous dichloromethane containing 0.2 mol·L^{-1} of [^{n}Bu$_4$N][B(C$_6$F$_5$)$_4$] as supporting electrolyte. The ESR spectra were recorded using an EMX X-Band ESR spectrometer, whereby the ESR spectrometer was triggered by a potentiostat, and the triggering was performed using the software package Potmaster v2 × 43.

Computational Part. Optimization of atomic coordinates was performed using the PBE functional[122] in the Priroda code.[123,124] The basis sets were TZ2P-quality {6s,3p,2d}/(11,6,2) for C and O, {3s,1p}/(5,1) for H, {10s,6p,2d}/(15,11,2) for S, and SBK-type core effective potentials with {5s,5p,4d}/(9,9,8) valence parts for Fe and Ru. Following the finding of Kaupp et al. on the suitable fraction of the exact exchange term for a reliable description of mixed-valence complexes,[93,102] calculations of all electronic properties reported here were performed using the B1LYP functional with an exact exchange term increased to 35%. These calculations were performed using the Orca suite[125−127] with ZORA scalar relativistic correction,[128] COSMO solvation correction for dichloromethane, and full-electron SARC-def2-TZVP[129] basis sets, including {311/1}/(5s1p) for H, {611111/411/11/1}/(11s6p2d1f) for C and O, {71111111/6111/21/1}/(14s9p3d1f) for S and P, {8111111111/611111/4111/1}/(17s11p7d1f) for Fe, and {811111111111/611111111/51111/1}/(19s14p9d1f) for Ru.

General Procedure: Synthesis of the 2,5-Bis(trimethylsilyl)-ethynyl Heterocycles 5 and 6. [PdCl$_2$(PPh$_3$)$_2$] (0.5 mol %) and [CuI] (6.0 mol %) were added to degassed ^{i}Pr$_2$NH (20 mL), and the mixture was stirred at ambient temperature for 10 min. Then, **3** or **4**, 2.1 equiv of trimethylsilylacetylene, and PPh$_3$ (6.0 mol %) were added, whereby the orange solution changed to dark brown. Within 10 min a precipitate formed and the reaction mixture was stirred overnight at 50 °C. The crude product was worked up by evaporation of the solvent, and the residue was dissolved in diethyl ether (50 mL) and filtered through a pad of Celite. The dark organic phase was evaporated, and the crude product was purified by sublimation (temperature: 50 °C, pressure: 5 mbar).

2,5-Bis(trimethylsilyl)furan (5). 2,5-Dibromofuran (6.0 g, 26.5 mmol), 0.5 mol % of [PdCl$_2$(PPh$_3$)$_2$] (196 mg, 0.28 mmol), 6.0 mol % of [CuI] (637 mg, 3.35 mmol), 6.0 mol % of PPh$_3$ (878 mg, 3.35 mmol), and 2.1 equiv of trimethylsilylacetylene (7.88 mL, 55.8 mmol) were used. Yield: 2.064 g (7.92 mmol, 30% based on 2,5-dibromofuran); colorless solid, soluble in hexane. Anal. Calcd for C$_{14}$H$_{20}$OSi$_2$ (260.48 g/mol) [%]: C, 64.55; H, 7.74. Found: C, 64.58; H, 7.83. Mp: 68 °C. ^{1}H NMR [CDCl$_3$, ppm] δ: 0.24 (s, 18 H, SiC$_3$H$_9$), 6.53 (s, 2 H, H-3/4). ^{13}C{^{1}H} NMR [CDCl$_3$, ppm] δ: −0.26 (SiC$_3$H$_9$), 93.80 (C$_4$NC≡CSi), 100.56 (C$_4$NC≡CSi), 116.43 (C-3/4), 137.48 (C-2/5). IR data [KBr, cm^{-1}] ν: 1502 (s, $\nu_{C=C}$), 2157 (s, $\nu_{C\equiv C}$), 2899 (w, $\nu_{s\text{-}CH3}$), 2963 (m, $\nu_{as\text{-}CH3}$), 3120, 3150 (w, $\nu_{=C-H}$). HR-ESI-MS [m/z]: calcd for C$_{14}$H$_{20}$OSi$_2$ 283.0945, found 283.0968 [M + Na]$^+$.

General Procedure: Synthesis of 2,5-((η^5-C$_5$H$_5$)(η^2-dppe)M-(C≡C)$_2$-^{c}C$_4$H$_2$E (E = O (11), S (12); M = Fe (a), Ru (b)). Compound **5** or **6** was dissolved in 30 mL of degassed methanol, and 2.3 equiv of K$_2$CO$_3$ was added in a single portion. The thus obtained reaction mixture was stirred overnight at ambient temperature. Then 2.2 equiv of [M(η^5-C$_5$H$_5$)(η^2-dppe)Cl] (**7**, M = Fe; **8**, M = Ru) and 2.3 equiv of [NH$_4$]PF$_6$ were added in a single portion, and the reaction mixture was refluxed for 3.5 h, whereby a color change from black to red (**7**) and from yellow to pale green (**8**) was observed. After cooling the reaction mixture to ambient temperature it was treated with 2.3 equiv of KO^{t}Bu, and stirring was continued for 30 min. The resulting precipitate was filtered off and washed with methanol (15 mL) and hexane (20 mL). The product was purified by crystallization from tetrahydrofuran at ambient temperature.

2,5-((η^5-C$_5$H$_5$)(η^2-dppe)FeC≡C)$_2$-^{c}C$_4$H$_2$O (11a). 2,5-Bis-(trimethylsilyl)ethynylfuran (**5**) (114 mg, 0.44 mmol), 2.3 equiv of K$_2$CO$_3$ (139 mg, 1.0 mmol), 2.2 equiv of **7** (534 mg, 0.96 mmol), 2.3 equiv of [NH$_4$]PF$_6$ (164 mg, 1.0 mmol), and 2.3 equiv of KO^{t}Bu (113 mg, 1.0 mmol) were used. Yield: 306 mg (0.26 mmol, 61% based on **5**); red solid, soluble in dichloromethane and tetrahydrofuran. Anal. Calcd for C$_{70}$H$_{60}$P$_4$Fe$_2$O (1152.81 g/mol) [%]: C, 72.93; H, 5.25. Found: C, 72.80; H, 5.33. Mp: 170 °C (dec). ^{1}H NMR [C$_6$D$_6$, ppm] δ: 1.92 (m, 4 H, CH$_2$-dppe), 2.60 (m, 4 H, CH$_2$-dppe), 4.24 (s, 10 H, C$_5$H$_5$), 5.75 (bs, 2 H, H-3/4), 6.95 (m, 8 H, C$_6$H$_5$/*o*-H), 7.01 (m, 4 H, C$_6$H$_5$/*p*-H), 7.13 (m, 8 H, C$_6$H$_5$/*m*-H), 7.16 (m, 4 H, C$_6$H$_5$/*p*-H), 7.21 (m, 8 H, C$_6$H$_5$/*o*-H), 8.01 (m, 8 H, C$_6$H$_5$/*m*-H). ^{13}C{^{1}H} NMR [C$_6$D$_6$, ppm] δ: 28.51−28.87 (dd, $^{1/2}J_{C-P} \approx$ 23 Hz, CH$_2$-dppe), 79.78 (s, C$_5$H$_5$), 108.44 (s, C-3/4), 111.80 (s, C-2/5), 117.57 (pt, $^2J_{C-P}$ = 25.33 Hz, FeC≡C), 127.85−127.92 (m, C$_6$H$_{5\text{-}m/m'}$), 128.71, 129.32 (s, C$_6$H$_{5\text{-}p/p'}$), 132.49, 134.06 (pt, $^2J_{C-P} \approx$ 4 Hz, C$_6$H$_{5\text{-}o/o'}$), 137.52 (s, FeC≡*C*), 138.91 (dt, $^1J_{C-P}$ = 24.8 Hz, $^4J_{C-P}$ = 5.8 Hz, C$_{i'}$-C$_6$H$_5$), 142.72 (dt, C$_i$-C$_6$H$_5$). ^{31}P{^{1}H} NMR [C$_6$D$_6$, ppm] δ: 119.58 (dppe). IR data [KBr, cm^{-1}] ν: 1093 (m, ν_{C-O}), 1432, 1482 (m, $\delta_{=C-H}$), 1547 (m, $\nu_{C=C}$), 2049 (s, $\nu_{C\equiv C}$), 3045 (w, $\nu_{=C-H}$). HR-ESI-MS [m/z]: calcd for C$_{70}$H$_{60}$P$_4$Fe$_2$O 1152.2292, found 1152.2290 [M]$^+$.

Crystal Data for 11a. Single crystals of **11a** were obtained by diffusion of hexane into a tetrahydrofuran solution containing **11a** at 25 °C. C$_{70}$H$_{60}$P$_4$Fe$_2$O, M_r = 1152.76 g·mol^{-1}, crystal dimensions 0.35 × 0.25 × 0.25 mm, monoclinic, $P2_1/c$, λ = 0.541 84 Å, a = 9.6703(2) Å, b = 25.2992(5) Å, c = 22.6350(5) Å, β = 94.250(2)°, V = 5522.4(2) Å^3, Z = 4, ρ_{calcd} = 1.386 g·cm^{-3}, μ = 5.661 mm^{-1}, T = 105 K, θ range =

DOI: 10.1021/acs.organomet.5b00104
Organometallics XXXX, XXX, XXX−XXX

3.49−67.50°, reflections collected 20 438, independent 9772, R_1 = 0.0477, wR_2 = 0.1215 [$I \geq 2\sigma(I)$].

2,5-((η⁵-C_5H_5)(η²-dppe)RuC≡C)$_2$-^{c}C_4H_2O (11b). 2,5-Bis(trimethylsilyl)ethynylfuran (**5**) (107 mg, 0.41 mmol), 2.3 equiv of K_2CO_3 (130 mg, 0.94 mmol), 2.2 equiv of **8** (542 mg, 0.90 mmol), 2.3 equiv of $[NH_4]PF_6$ (154 mg, 0.94 mmol), and 2.3 equiv of KO^{t}Bu (106 mg, 0.94 mmol) were used. Yield: 258 mg (0.21 mmol, 50% based on **5**); pale green solid, soluble in dichloromethane and tetrahydrofuran. Anal. Calcd for $C_{70}H_{60}P_4Ru_2O$ (1243.26 g/mol) [%]: C, 67.62; H, 4.86. Found: C, 67.37; H, 4.86. Mp: 145 °C (dec). ^{1}H NMR [C_6D_6, ppm] δ: 1.96 (m, 4 H, CH_2-dppe), 2.61 (m, 4 H, CH_2-dppe), 4.69 (s, 10 H, C_5H_5), 5.70 (s, 2 H, H-3/4), 6.93−7.00 (m, 16 H, C_6H_5), 7.18−7.24 (m, 16 H, C_6H_5), 7.99 (m, 8 H, C_6H_5/*m*-H). ^{13}C{^{1}H} NMR [C_6D_6, ppm] δ: 28.30−28.67 (dd, $^{1/2}J_{C-P}$ ≈ 22.95 Hz,CH_2-dppe), 83.06 (s, C_5H_5), 103.36 (s, C-2/5), 108.77 (s, C-3/4), 117.65 (pt, $^2J_{C-P}$ = 25.37 Hz, RuC≡C), 127.87−127.96 (m, C_6H_5-$_{m/m'}$), 128.82, 129.45 (s, C_6H_5-$_{p/p'}$), 132.26, 134.26 (pt, $^2J_{C-P}$ ≈ 5.2 Hz, C_6H_5-$_{o/o'}$), 138.23 (dt, $^1J_{C-P}$ = 27.3 Hz, $^4J_{C-P}$ = 3.6 Hz, C_i-C_6H_5), 139.27 (s, RuC≡C), 142.93 (dt, $^1J_{C-P}$ = 25.8 Hz, $^4J_{C-P}$ = 9.0 Hz, $C_{i'}$-C_6H_5). ^{31}P{^{1}H} NMR [C_6D_6, ppm] δ: 98.76 (dppe). IR data [KBr, cm^{-1}] ν: 1095 (m, ν_{C-O}), 1431, 1482 (m, $\delta_{=C-H}$), 1549 (m, $\nu_{C=C}$), 2062 (s, $\nu_{C\equiv C}$), 3044 (w, $\nu_{=C-H}$). HR-ESI-MS [*m*/*z*]: calcd for $C_{70}H_{60}P_4Ru_2O$ 1244.1680, found 1244.1682 [M]$^+$.

2,5-((η⁵-C_5H_5)(η²-dppe)FeC≡C)$_2$-^{c}C_4H_2S (12a). 2,5-Bis(trimethylsilyl)ethynylthiophene (**6**) (50 mg, 0.18 mmol), 2.3 equiv of K_2CO_3 (57 mg, 0.42 mmol), 2.2 equiv of **7** (220 mg, 0.40 mmol), 2.3 equiv of $[NH_4]PF_6$ (68 mg, 0.42 mmol), and 2.3 equiv of KO^{t}Bu (47 mg, 0.24 mmol) were used. Yield: 113 mg (0.09 mmol, 54% based on **6**); red solid, soluble in dichloromethane and tetrahydrofuran. Anal. Calcd for $C_{70}H_{60}P_4Fe_2S$ (1168.88 g/mol) [%]: C, 71.93; H, 5.17. Found: C, 71.49; H, 5.23. Mp: 210 °C (dec). ^{1}H NMR [C_6D_6, ppm] δ: 1.88 (m, 4 H, CH_2-dppe), 2.52 (m, 4 H, CH_2-dppe), 4.21 (s, 10 H, C_5H_5), 6.29 (bs, 2 H, H-3/4), 6.96 (m, 8 H, C_6H_5/*o*-H), 7.01 (m, 4 H, C_6H_5/*p*-H), 7.16 (m, 8 H, C_6H_5/*m*-H), 7.20 (m, 4 H, C_6H_5/*p*-H), 7.26 (m, 8 H, C_6H_5/*o*-H), 7.97 (m, 8 H, C_6H_5/*m*-H). ^{13}C{^{1}H} NMR [C_6D_6, ppm] δ: 28.49−28.86 (dd, $^{1/2}J_{C-P}$ ≈ 23 Hz,CH_2-dppe), 79.61 (s, C_5H_5), 114.31 (s, C-2/5), the signal for FeC≡C could not be detected, 124.85 (s, C-3/4), 127.92 (m, C_6H_5-$_{m/m'}$), 128.74, 129.32 (s, C_6H_5-$_{p/p'}$), 132.46, 134.01 (pt, $^2J_{C-P}$ ≈ 4.2 Hz, C_6H_5-$_{o/o'}$), 138.97 (dt, $^1J_{C-P}$ = 23.7 Hz, $^4J_{C-P}$ = 4.3 Hz, C_i-C_6H_5), 139.64 (s, FeC≡C), 142.84 (dt, $C_{i'}$-C_6H_5). ^{31}P{^{1}H} NMR [C_6D_6, ppm] δ: 119.72 (dppe). IR data [KBr, cm^{-1}] ν: 1431, 1480 (m, $\delta_{=C-H}$), 1500 (m, $\nu_{C=C}$), 2044 (s, $\nu_{C\equiv C}$), 3046 (w, $\nu_{=C-H}$). HR-ESI-MS [*m*/*z*]: calcd for $C_{70}H_{60}P_4Fe_2S$ 1168.2064, found 1168.2019 [M]$^+$.

Crystal Data for 12a. Single crystals of **12a** were obtained by diffusion of toluene into a dichloromethane solution containing **12a** at 25 °C. $C_{70}H_{60}P_4Fe_2S$, M_r = 1168.82 g·mol^{-1}, crystal dimensions 0.30 × 0.20 × 0.09 mm, monoclinic, $P2_1/c$, λ = 0.710 73 Å, *a* = 9.8267(2) Å, *b* = 25.4997(5) Å, *c* = 22.3763(6) Å, β = 92.369(2)°, *V* = 5602.2(2) Å^3, *Z* = 4, ρ_{calcd} = 1.386 g·cm^{-3}, μ = 0.714 mm^{-1}, *T* = 107 K, θ range = 2.93−26.00°, reflections collected 27 913, independent 10 947, R_1 = 0.0548, wR_2 = 0.1217 [$I \geq 2\sigma(I)$].

2,5-((η⁵-C_5H_5)(η²-dppe)RuC≡C)$_2$-^{c}C_4H_2S (12b). 2,5-Bis(trimethylsilyl)ethynylthiophene (**6**) (113 mg, 0.41 mmol), 2.3 equiv of K_2CO_3 (130 mg, 0.94 mmol), 2.2 equiv of **8** (539 mg, 0.90 mmol), 2.3 equiv of $[NH_4]PF_6$ (153 mg, 0.94 mmol), and 2.3 equiv of KO^{t}Bu (105 mg, 0.94 mmol) were used. Yield: 360 mg (0.29 mmol, 70% based on **6**); pale green solid, soluble in dichloromethane and tetrahydrofuran. Anal. Calcd for $C_{70}H_{60}P_4Ru_2S$ (1259.33 g/mol) [%]: C, 66.76; H, 4.80. Found: C, 66.77; H, 4.90. Mp: 210 °C (dec). ^{1}H NMR [C_6D_6, ppm] δ: 1.93 (m, 4 H, CH_2-dppe), 2.55 (m, 4 H, CH_2-dppe), 4.67 (s, 10 H, C_5H_5), 6.26 (s, 2 H, H-3/4), 6.95−7.00 (m, 16 H, C_6H_5), 7.20−7.29 (m, 16 H, C_6H_5), 7.96 (m, 8 H, C_6H_5/*m*-H). ^{13}C{^{1}H} NMR [C_6D_6, ppm] δ: 28.20−28.57 (dd, $^{1/2}J_{C-P}$ ≈ 22.95 Hz, CH_2-dppe), 82.89 (s, C_5H_5), 105.52 (s, C-2/5), 117.63 (pt, $^2J_{C-P}$ = 25.62 Hz, RuC≡C), 125.27 (s, C-3/4), 127.50−127.75 (m, C_6H_5-$_{m/m'}$), 128.83, 129.45 (s, C_6H_5-$_{p/p'}$), 132.26 (pt, $^2J_{C-P}$ ≈ 5.0 Hz, C_6H_5-$_o$), 133.10 (s, RuC≡C), 134.19 (pt, $^2J_{C-P}$ ≈ 5.3 Hz, C_6H_5-$_{o'}$), 138.20 (dt, $^1J_{C-P}$ = 28.3 Hz, $^4J_{C-P}$ = 4.4 Hz, C_i-C_6H_5), 143.00 (dt, $^1J_{C-P}$ = 25.3 Hz, $^4J_{C-P}$ = 8.6 Hz, $C_{i'}$-C_6H_5). ^{31}P{^{1}H} NMR [C_6D_6, ppm] δ: 98.74 (dppe). IR data [KBr, cm^{-1}] ν: 1433, 1478 (m, $\delta_{=C-H}$), 1500 (m, $\nu_{C=C}$), 2053 (s, $\nu_{C\equiv C}$), 3047 (w, $\nu_{=C-H}$). HR-ESI-MS [*m*/*z*]: calcd for $C_{70}H_{60}P_4Ru_2S$ 1260.1452, found 1260.1410 [M]$^+$.

Crystal Data for 12b. Single crystals of **12b** were obtained by diffusion of toluene into a dichloromethane solution containing **12b** at 25 °C. $C_{70}H_{60}P_4Ru_2S$, M_r = 1259.26 g·mol^{-1}, crystal dimensions 0.38 × 0.30 × 0.20 mm, monoclinic, $P2_1/c$, λ = 0.710 73 Å, *a* = 16.8002(5) Å, *b* = 15.7240(4) Å, *c* = 22.0975(7) Å, β = 104.717(3)°, *V* = 5645.9(3) Å^3, *Z* = 4, ρ_{calcd} = 1.481 g·cm^{-3}, μ = 0.729 mm^{-1}, *T* = 293 K, θ range = 2.85−25.68°, reflections collected 39 855, independent 10 684, R_1 = 0.0495, wR_2 = 0.1306 [$I \geq 2\sigma(I)$].

General Procedure: Synthesis of 15 and 16. 2-(Trimethylsilyl)ethynylthiophene (**13**) or 2-(trimethylsilyl)ethynyl-5-methylthiophene (**14**) was dissolved in 30 mL of degassed methanol, and 2.3 equiv of K_2CO_3 was added in a single portion. The thus obtained reaction mixture was stirred overnight at ambient temperature. Then 2.2 equiv of [Ru(η⁵-C_5H_5)(η²-dppe)Cl] (**8**) and 2.3 equiv of $[NH_4]PF_6$ were added in a single portion, and the reaction mixture was refluxed for 3.5 h. After cooling the reaction mixture to ambient temperature it was treated with 2.3 equiv of KO^{t}Bu, and stirring was continued for 2 h. The resulting precipitate was filtered off and washed with methanol (15 mL) and hexane (20 mL). The product was dried in an oil pump vacuum.

2-((η⁵-C_5H_5)(η²-dppe)RuC≡C)-^{c}C_4H_3S (15). 2-(Trimethylsilyl)ethynylthiophene (**13**) (60 mg, 0.33 mmol), 1.3 equiv of K_2CO_3 (60 mg, 0.43 mmol), 1 equiv of **8** (200 mg, 0.33 mmol), 1.3 equiv of $[NH_4]PF_6$ (71 mg, 0.43 mmol), and 1.3 equiv of KO^{t}Bu (48 mg, 0.43 mmol) were used. Yield for $C_{37}H_{32}P_2RuS$ (671.73 g/mol): 115 mg (0.17 mmol, 51% based on **13**); yellow solid, soluble in dichloromethane and tetrahydrofuran. Mp: 218 °C. ^{1}H NMR [C_6D_6, ppm] δ: 1.92−2.03 (m, 2 H, CH_2-dppe), 2.49−2.60 (m, 2 H, CH_2-dppe), 4.70 (s, 5 H, C_5H_5), 6.50−6.51 (m, 2 H, H-3/5), 6.63 (dd, 1 H, $^3J_{H-H}$ = 5.0 Hz, $^4J_{H-H}$ = 3.7 Hz, H-4), 6.96−7.00 (m, 6 H, C_6H_5), 7.19−7.23 (m, 6 H, C_6H_5), 7.30 (m, 4 H, C_6H_5/*p*-H), 7.98 (m, 4 H, C_6H_5/*m*-H). ^{13}C{^{1}H} NMR [C_6D_6, ppm] δ: 28.25−28.62 (dd, $^{1/2}J_{C-P}$ ≈ 23 Hz,CH_2-dppe), 83.00 (s, C_5H_5), 104.30 (s, C-2), 120.22 (s, C-5), 122.25 (pt, $^2J_{C-P}$ = 25.5 Hz, RuC≡C), 125.39 (s, C-3), 126.19 (s, C-4), 127.96−128.04 (m, C_6H_5-$_{o/m}$), 128.94, 129.60 (s, C_6H_5-$_{p/p'}$), 132.05 (pt, $^2J_{C-P}$ ≈ 5.4 Hz, C_6H_5-$_{o'}$), 132.56 (pt, $^3J_{C-P}$ = 1.6 Hz, RuC≡C), 134.29 (pt, $^2J_{C-P}$ ≈ 5.2 Hz, C_6H_5-$_{m'}$), 137.80 (dt, $^1J_{C-P}$ = 28.0 Hz, $^4J_{C-P}$ = 4.5 Hz, C_i-C_6H_5), 142.91 (dt, $^1J_{C-P}$ = 26.5 Hz, $^4J_{C-P}$ = 9.7 Hz, $C_{i'}$-C_6H_5). ^{31}P{^{1}H} NMR [C_6D_6, ppm] δ: 98.95 (dppe). IR data [KBr, cm^{-1}] ν: 1091 (s, ν_{C-C}), 1432, 1481 (m, $\delta_{=C-H}$), 1571, 1582 (w, $\nu_{C=C}$), 2069 (s, $\nu_{C\equiv C}$), 2903, 2923 (w, $\nu_{s\text{-}CH3}$), 2984 (w, $\nu_{as\text{-}CH3}$), 3048 (w, $\nu_{=C-H}$). HR-ESI-MS [*m*/*z*]: calcd for $C_{37}H_{32}P_2RuS$ 672.0747, found 672.0743 [M]$^+$; calcd 695.0645, found 695.0599 [M + *n*Na]$^+$.

2-((η⁵-C_5H_5)(η²-dppe)RuC≡C)-5-methyl-^{c}C_4H_2S (16). 2-(Trimethylsilyl)ethynyl-5-methyl thiophene (**14**) (63 mg, 0.32 mmol), 1.3 equiv of K_2CO_3 (58 mg, 0.42 mmol), 1 equiv of **8** (194 mg, 0.32 mmol), 1.3 equiv of $[NH_4]PF_6$ (68 mg, 0.42 mmol), and 1.3 equiv of KO^{t}Bu (47 mg, 0.42 mmol) were used. Yield for $C_{38}H_{34}P_2RuS$ (685.76 g/mol): 110 mg (0.16 mmol, 49% based on **13**); yellow solid, soluble in dichloromethane and tetrahydrofuran. Mp: 206 °C. ^{1}H NMR [C_6D_6, ppm] δ: 1.96−2.03 (m, 2 H, CH_2-dppe), 2.07 (d, 3 H, $^4J_{H-H}$ = 0.8 Hz, CH_3), 2.55−2.62 (m, 2 H, CH_2-dppe), 4.71 (s, 5 H, C_5H_5), 6.34 (dd, 1 H, $^3J_{H-H}$ = 3.4 Hz, $^4J_{H-H}$ = 1.1 Hz, H-4), 6.39 (d, 1 H, $^3J_{H-H}$ = 3.4 Hz, H-3), 6.95−6.98 (m, 6 H, C_6H_5), 7.20−7.23 (m, 6 H, C_6H_5), 7.31 (m, 4 H, C_6H_5/*p*-H), 8.00 (m, 4 H, C_6H_5/*m*-H). ^{13}C{^{1}H} NMR [C_6D_6, ppm] δ: 15.36 (s, CH_3), 28.26−28.63 (dd, $^{1/2}J_{C-P}$ ≈ 23 Hz,CH_2-dppe), 82.98 (s, C_5H_5), 104.78 (s, C-2), 120.09 (pt, $^2J_{C-P}$ = 25.6 Hz, RuC≡C), 124.34 (s, C-4), 125.49 (s, C-3), 127.95−128.05 (m, C_6H_5-$_{o/m}$), 128.90, 129.58 (s, C_6H_5-$_{p/p'}$), 130.67 (pt, $^3J_{C-P}$ = 1.6 Hz, RuC≡C), 132.08 (pt, $^2J_{C-P}$ = 5.3 Hz, C_6H_5-$_{o'}$), 133.94 (s, C-5), 134.32 (pt, $^3J_{C-P}$ = 5.1 Hz,C_6H_5-$_{m'}$), 137.95 (dt, $^1J_{C-P}$ = 28.2 Hz, $^4J_{C-P}$ = 4.6 Hz, C_i-C_6H_5), 143.00 (dt, $^1J_{C-P}$ = 26.4 Hz, $^4J_{C-P}$ = 9.6 Hz, $C_{i'}$-C_6H_5). ^{31}P{^{1}H} NMR [C_6D_6, ppm] δ: 99.03 (dppe). IR data [KBr, cm^{-1}] ν: 1091 (s, ν_{C-C}), 1433, 1480 (m, $\delta_{=C-H}$), 1585 (w, $\nu_{C=C}$), 2065 (s, $\nu_{C\equiv C}$), 2848 (w, $\nu_{s\text{-}CH3}$),

DOI: 10.1021/acs.organomet.5b00104
Organometallics XXXX, XXX, XXX−XXX

2913 (w, $\nu_{as\text{-}CH_3}$), 3049 (w, $\nu_{=C-H}$). HR-ESI-MS [m/z]: calcd for $C_{38}H_{34}P_2RuS$ 686.0904, found 686.0892 $[M]^+$.

■ ASSOCIATED CONTENT

Supporting Information

ORTEP diagrams of **11a** and **12a,b**; UV−vis/NIR spectra and their deconvolution (**11b** and **12a,b**); IR spectra (spectroelectrochemistry) of **11b** and **12a,b**; data for DFT and spin density. Crystallographic data of **11a** and **12a,b** are also available from the Cambridge Crystallographic Database as file numbers CCDC 1023501 (**11a**), 1023360 (**12a**), and 1023358 (**12b**). The Supporting Information is available free of charge on the ACS Publications website at DOI: 10.1021/acs.organomet.5b00104.

■ AUTHOR INFORMATION

Corresponding Author

*E-mail: heinrich.lang@chemie.tu-chemnitz.de. Phone: +49 (0) 371-531-21210. Fax: +49 (0)371-531-21219.

Notes

The authors declare no competing financial interest.

■ ACKNOWLEDGMENTS

We are grateful to the Fonds der Chemischen Industrie (FCI) for generous financial support. M.K. and D.S. thank the FCI for a Ph.D. fellowship. We thank Dipl.-Chem. J. M. Speck for fruitful discussions. Dedicated to Prof. Dr. Stefan Spange on the occasion of his 65th birthday.

■ REFERENCES

(1) Low, P. J. *Coord. Chem. Rev.* **2013**, *257*, 1507−1532.
(2) Bruce, M. I. *Coord. Chem. Rev.* **2004**, *248*, 1603−1625.
(3) Costuas, K.; Rigaut, S. *Dalton Trans.* **2011**, *40*, 5643−5658.
(4) Carroll, R. L.; Gorman, C. B. *Angew. Chem., Int. Ed.* **2002**, *41*, 4378−4400.
(5) McCleverty, J. A.; Ward, M. D. *Acc. Chem. Res.* **1998**, *31*, 842−851.
(6) Sukegawa, J.; Schubert, C.; Zhu, X.; Tsuji, H.; Guldi, D. M.; Nakamura, E. *Nat. Chem.* **2014**, *6*, 899−905.
(7) Burgun, A.; Ellis, B. G.; Roisnel, T.; Skelton, B. W.; Bruce, M. I.; Lapinte, C. *Organometallics* **2014**, *33*, 4209−4219.
(8) Wuttke, E.; Hervault, Y.; Polit, W.; Linseis, M.; Erler, P.; Winter, R. F. *Organometallics* **2013**, *33*, 4672−4686.
(9) Rigaut, S. *Dalton Trans.* **2013**, *42*, 15859−15863.
(10) Schwarz, F.; Kastlunger, G.; Lissel, F.; Riel, H.; Venkatesan, K.; Berke, H.; Stadler, R.; Lörtscher, E. *Nano Lett.* **2014**, *14*, 5932−5940.
(11) Lissel, F.; Schwarz, F.; Blacque, O.; Riel, H.; Lörtscher, E.; Venkatesan, K.; Berke, H. *J. Am. Chem. Soc.* **2014**, *136*, 14560−14569.
(12) Marqués-González, S.; Yufit, D. S.; Howard, J. A. K.; Martín, S.; Osorio, H. M.; García-Suárez, V. M.; Nichols, R. J.; Higgins, S. J.; Cea, P.; Low, P. J. *Dalton Trans.* **2013**, 338−341.
(13) Lang, H.; George, D. S.; Rheinwald, G. *Coord. Chem. Rev.* **2000**, *206−207*, 101−197.
(14) Lang, H.; Packheiser, R.; Walfort, B. *Organometallics* **2006**, *25*, 1836−1850.
(15) Frosch, W.; Back, S.; Rheinwald, G.; Köhler, K.; Pritzkow, H.; Lang, H. *Organometallics* **2000**, *19*, 4016−4024.
(16) Justaud, F.; Roisnel, T.; Lapinte, C. *New J. Chem.* **2011**, *35*, 2219−2226.
(17) De Montigny, F.; Argouarch, G.; Costuas, K.; Halet, J.-F.; Roisnel, T.; Toupet, L.; Lapinte, C. *Organometallics* **2005**, *24*, 4558−4572.
(18) Costuas, K.; Cador, O.; Justaud, F.; Le Stang, S.; Paul, F.; Monari, A.; Evangelisti, S.; Toupet, L. C.; Lapinte, C.; Halet, J.-F. *Inorg. Chem.* **2011**, *50*, 12601−12622.
(19) Lohan, M.; Justaud, F.; Lang, H.; Lapinte, C. *Organometallics* **2012**, *31*, 3565−3574.
(20) Schauer, P. A.; Low, P. J. *Eur. J. Inorg. Chem.* **2012**, *2012*, 390−411.
(21) Khairul, W. M.; Fox, M. A.; Schauer, P. A.; Albesa-Jové, D.; Yufit, D. S.; Howard, J. A. K.; Low, P. J. *Inorg. Chim. Acta* **2011**, *374*, 461−471.
(22) Long, E. M.; Brown, N. J.; Man, W. Y.; Fox, M. A.; Yufit, D. S.; Howard, J. A. K.; Low, P. J. *Inorg. Chim. Acta* **2012**, *380*, 358−371.
(23) Bruce, M. I.; Kramarczuk, K. A.; Skelton, B. W.; White, A. H. *J. Organomet. Chem.* **2010**, *695*, 469−473.
(24) Bruce, M. I.; Fox, M. A.; Low, P. J.; Nicholson, B. K.; Parker, C. R.; Patalinghug, W. C.; Skelton, B. W.; White, A. H. *Organometallics* **2012**, *31*, 2639−2657.
(25) Bruce, M. I.; Costuas, K.; Davin, T.; Halet, J.-F.; Kramarczuk, K. A.; Low, P. J.; Nicholson, B. K.; Perkins, G. J.; Roberts, R. L.; Skelton, B. W.; Smith, M. E.; White, A. H. *Dalton Trans.* **2007**, 5387−5399.
(26) Bruce, M. I.; Kramarczuk, K. A.; Skelton, B. W.; White, A. H. *J. Organomet. Chem.* **2010**, *695*, 469−473.
(27) Fitzgerald, E. C.; Brown, N. J.; Edge, R.; Helliwell, M.; Roberts, H. N.; Tuna, F.; Beeby, A.; Collison, D.; Low, P. J.; Whiteley, M. W. *Organometallics* **2012**, *31*, 157−169.
(28) Coat, F.; Paul, F.; Lapinte, C.; Toupet, L.; Costuas, K.; Halet, J.-F. *J. Organomet. Chem.* **2003**, *683*, 368−378.
(29) Fitzgerald, E. C.; Ladjarafi, A.; Brown, N. J.; Collison, D.; Costuas, K.; Edge, R.; Halet, J.-F.; Justaud, F.; Low, P. J.; Meghezzi, H.; Roisnel, T.; Whiteley, M. W.; Lapinte, C. *Organometallics* **2011**, *30*, 4180−4195.
(30) Quardokus, R. C.; Lu, Y.; Wasio, N. A.; Lent, C. S.; Justaud, F.; Lapinte, C.; Kandel, S. A. *J. Am. Chem. Soc.* **2012**, *134*, 1710−1714.
(31) Tanaka, Y.; Shaw-Taberlet, J. A.; Justaud, F.; Cador, O.; Roisnel, T.; Akita, M.; Hamon, J.-R.; Lapinte, C. *Organometallics* **2009**, *28*, 4656−4669.
(32) Fox, M. A.; Le Guennic, B.; Roberts, R. L.; Brue, D. A.; Yufit, D. S.; Howard, J. A. K.; Manca, G.; Halet, J.-F.; Hartl, F.; Low, P. J. *J. Am. Chem. Soc.* **2011**, *133*, 18433−18446.
(33) Brown, N. J.; Lancashire, H. N.; Fox, M. A.; Collison, D.; Edge, R.; Yufit, D. S.; Howard, J. A. K.; Whiteley, M. W.; Low, P. J. *Organometallics* **2011**, *30*, 884−894.
(34) Xia, J.-L.; Man, W. Y.; Zhu, X.; Zhang, C.; Jin, G.-J.; Schauer, P. A.; Fox, M. A.; Yin, J.; Yu, G.-A.; Low, P. J.; Liu, S. H. *Organometallics* **2012**, *31*, 5321−5333.
(35) Lohan, M.; Justaud, F.; Roisnel, T.; Ecorchard, P.; Lang, H.; Lapinte, C. *Organometallics* **2010**, *29*, 4804−4817.
(36) Lohan, M.; Ecorchard, P.; Rüffer, T.; Justaud, F.; Lapinte, C.; Lang, H. *Organometallics* **2009**, *28*, 1878−1890.
(37) Dong, T.-Y.; Lin, S.-F.; Chen, C.-P.; Yeh, S.-W.; Chen, H.-Y.; Wen, Y.-S. *J. Organomet. Chem.* **2009**, *694*, 1529−1541.
(38) Kheradmandan, S.; Venkatesan, K.; Blacque, O.; Schmalle, H. W.; Berke, H. *Chem.—Eur. J.* **2004**, *10*, 4872−4885.
(39) Dembinski, R.; Lis, T.; Szafert, S.; Mayne, C. L.; Bartik, T.; Gladysz, J. A. *J. Organomet. Chem.* **1999**, *578*, 229−246.
(40) Dembinski, R.; Bartik, T.; Bartik, B.; Jaeger, M.; Gladysz, J. A. *J. Am. Chem. Soc.* **2000**, *122*, 810−822.
(41) Goetsch, W. R.; Solntsev, P. V.; Van Stappen, C.; Purchel, A. A.; Dudkin, S. V.; Nemykin, V. N. *Organometallics* **2014**, *33*, 145−157.
(42) Sato, M.-A.; Fukui, K. *Synth. Met.* **2007**, *157*, 619−626.
(43) Sato, M.; Fukui, K.; Sakamoto, M.; Kashiwagi, S.; Hiroi, M. *Thin Solid Films* **2001**, *393*, 210−216.
(44) Bildstein, B.; Malaun, M.; Kopacka, H.; Wurst, K.; Mitterböck, M.; Ongania, K.; Opromolla, G.; Zanello, P. *Organometallics* **1999**, *18*, 4325−4336.
(45) Hildebrandt, A.; Schaarschmidt, D.; Claus, R.; Lang, H. *Inorg. Chem.* **2011**, 10623−10632.
(46) Speck, J. M.; Claus, R.; Hildebrandt, A.; Rüffer, T.; Erasmus, E.; van As, L.; Swarts, J. C.; Lang, H. *Organometallics* **2012**, *31*, 6373−6380.
(47) Hildebrandt, A.; Schaarschmidt, D.; Lang, H. *Organometallics* **2011**, *30*, 556−563.

DOI: 10.1021/acs.organomet.5b00104
Organometallics XXXX, XXX, XXX−XXX

(48) Hildebrandt, A.; Lang, H. *Organometallics* **2013**, *32*, 5640−5653.
(49) Miesel, D.; Hildebrandt, A.; Korb, M.; Low, P. J.; Lang, H. *Organometallics* **2013**, *32*, 2993−3002.
(50) Lehrich, S. W.; Hildebrandt, A.; Rüffer, T.; Korb, M.; Low, P. J.; Lang, H. *Organometallics* **2014**, *33*, 4836−4845.
(51) Kaleta, K.; Strehler, F.; Hildebrandt, A.; Beweries, T.; Arndt, P.; Rüffer, T.; Spannenberg, A.; Lang, H.; Rosenthal, U. *Chem.—Eur. J.* **2012**, *18*, 12672−12680.
(52) Kaleta, K.; Hildebrandt, A.; Strehler, F.; Arndt, P.; Jiao, H.; Spannenberg, A.; Lang, H.; Rosenthal, U. *Angew. Chem., Int. Ed.* **2011**, *50*, 11248−11252.
(53) Hildebrandt, A.; Pfaff, U.; Lang, H. *Rev. Inorg. Chem.* **2011**, *31*, 111−141.
(54) Robin, M. B.; Day, P. *Adv. Inorg. Chem. Radiochem.* **1967**, *10*, 247−422.
(55) Le Stang, S.; Paul, F.; Lapinte, C. *Organometallics* **2000**, *19*, 1035−1043.
(56) Ou, Y.-P.; Xia, J.; Zhang, J.; Xu, M.; Yin, J.; Yu, G.-A.; Liu, S. H. *Chem.—Asian J.* **2013**, *8*, 2023−2032.
(57) Hesse, M.; Meier, H.; Zeeh, B. *Spektroskopische Methoden der Organischen Chemie*, 7th ed.; Thieme: Stuttgart, 2005; p 9.
(58) Metzinger, H. G. *Org. Magn. Reson.* **1971**, *3*, 485−494.
(59) Harris, R. K. *Can. J. Chem.* **1964**, *42*, 2275−2281.
(60) Lang, H.; Blau, S.; Rheinwald, G. *J. Organomet. Chem.* **1995**, *492*, 81−85.
(61) Smith, M. B.; March, J. *March's Advanced Organic Chemistry: Reactions, Mechanisms, and Structure*, 5th ed.; Wiley-VCH: New York, 2001; pp 20−36.
(62) Li, P.; Ahrens, B.; Choi, K.-H.; Khan, M. S.; Raithby, P. R.; Wilson, P. J.; Wong, W.-Y. *CrystEngComm* **2002**, *4*, 405−412.
(63) Lewis, J.; Long, N. J.; Raithby, P. R.; Shields, G. P.; Wong, W.-Y.; Younus, M. *J. Chem. Soc., Dalton Trans.* **1997**, 4283−4288.
(64) Wong, W.-Y.; Choi, K.-H.; Lu, G.-L.; Lin, Z. *Organometallics* **2002**, *21*, 4475−4481.
(65) A CCDC database search for 2,5-bis(metalloethynyl)-substituted five-membered heterocycles (MC≡C-C_4H_2E; E = O, S, N; M = any transition metal) results in the discussed *end-on* derivatives, but also compounds bearing the metals coordinated *side-on* at the C≡C bond, which are listed for the sake of completeness. This results in tetra- or octahedral structures, and thus, enlarged C≡C bonds are present (C_2M_2 (M = Co) tetrahedron, 1.375(8) Å; $C_2M'_2M_2$ (M ≠ M′ = Mo, Ir, W) octahedron 1.449(9) to 1.507(15) Å). Arnanz, A.; Marcos, M.-L.; Moreno, C.; Farrar, D. H.; Lough, A. J.; Yu, J. O.; Delgado, S.; González-Velasco, J. *J. Organomet. Chem.* **2004**, *689*, 3218−3231. Lucas, N. T.; Humphrey, M. G.; Willis, A. C. *Acta Crystallogr., Sect. E Struct. Rep. Online* **2005**, *61*, m463−m464. Notaras, E. G. A.; Lucas, N. T.; Humphrey, M. G.; Willis, A. C.; Rae, A. D. *Organometallics* **2003**, *22*, 3659−3670.
(66) Bruce, M. I.; Hall, B. C.; Kelly, B. D.; Low, P. J.; Skelton, B. W.; White, A. H. *J. Chem. Soc., Dalton Trans.* **1999**, 3719−3728.
(67) Bruce, M. I.; Low, P. J.; Skelton, B. W.; White, A. H. *New J. Chem.* **1998**, *22*, 419−422.
(68) Bruce, M. I.; Hinterding, P.; Tiekink, E. R. T.; Skelton, B. W.; White, A. H. *J. Organomet. Chem.* **1993**, *450*, 209−218.
(69) Gao, L.-B.; Zhang, L.-Y.; Shi, L.-X.; Chen, Z.-N. *Organometallics* **2005**, *24*, 1678−1684.
(70) Bruce, M. I.; Ellis, B. G.; Gaudio, M.; Lapinte, C.; Melino, G.; Paul, F.; Skelton, B. W.; Smith, M. E.; Toupet, L.; White, A. H. *Dalton Trans.* **2004**, 1601−1609.
(71) Bruce, M. I.; Kelly, B. D.; Skelton, B. W.; White, A. H. *J. Organomet. Chem.* **2000**, *604*, 150−156.
(72) Ge, Q.; Dalton, G. T.; Humphrey, M. G.; Samoc, M.; Hor, T. S. A. *Chem.—Asian J.* **2009**, *4*, 998−1005.
(73) Bruce, M. I.; Low, P. J.; Hartl, F.; Humphrey, P. A.; de Montigny, F.; Jevric, M.; Lapinte, C.; Perkins, G. J.; Roberts, R. L.; Skelton, B. W.; White, A. H. *Organometallics* **2005**, *24*, 5241−5255.
(74) Barrière, F.; Geiger, W. E. *J. Am. Chem. Soc.* **2006**, *128*, 3980−3989.
(75) Chong, D.; Slote, J.; Geiger, W. E. *J. Electroanal. Chem.* **2009**, *630*, 28−34.
(76) Pfaff, U.; Hildebrandt, A.; Schaarschmidt, D.; Rüffer, T.; Low, P. J.; Lang, H. *Organometallics* **2013**, *32*, 6106−6117.
(77) Hildebrandt, A.; Lang, H. *Organometallics* **2013**, *32*, 5640−5653.
(78) LeSuer, R. J.; Buttolph, C.; Geiger, W. E. *Anal. Chem.* **2004**, *76*, 6395−6401.
(79) Gericke, H. J.; Barnard, N. I.; Erasmus, E.; Swarts, J. C.; Cook, M. J.; Aquino, M. a. S. *Inorg. Chim. Acta* **2010**, *363*, 2222−2232.
(80) Nemykin, V. N.; Rohde, G. T.; Barrett, C. D.; Hadt, R. G.; Sabin, J. R.; Reina, G.; Galloni, P.; Floris, B. *Inorg. Chem.* **2010**, *49*, 7497−7509.
(81) Gritzner, G.; Kuta, J. *Pure Appl. Chem.* **1984**, *56*, 461−466.
(82) Sato, M.; Kubota, Y.; Tanemura, A.; Maruyama, G.; Fujihara, T.; Nakayama, J.; Takayanagi, T.; Takahashi, K.; Unoura, K. *Eur. J. Inorg. Chem.* **2006**, *2006*, 4577−4588.
(83) Connelly, N. G.; Geiger, W. E. *Chem. Rev.* **1996**, *96*, 877−910.
(84) Halet, J.-F.; Lapinte, C. *Coord. Chem. Rev.* **2013**, *257*, 1584−1613.
(85) Bruce, M. I.; Costuas, K.; Davin, T.; Ellis, B. G.; Halet, J. F.; Lapinte, C.; Low, P. J.; Smith, M. E.; Skelton, B. W.; Toupet, L.; White, A. H. *Organometallics* **2005**, *24*, 3864−3881.
(86) Tanaka, Y.; Ishisaka, T.; Koike, T.; Akita, M. *Polyhedron* **2015**, *86*, 105−110.
(87) Krejčik, M.; Daněk, M.; Hartl, F. *J. Electroanal. Chem.* **1991**, *317*, 179−187.
(88) Demadis, K. D.; Hartshorn, C. M.; Meyer, T. J. *Chem. Rev.* **2001**, *101*, 2655−2686.
(89) Hush, N. S. *Electrochim. Acta* **1968**, *13*, 1005−1023.
(90) Hush, N. S. *Prog. Inorg. Chem.* **1967**, *8*, 391−444.
(91) D'Alessandro, D. M.; Keene, F. R. *Chem. Soc. Rev.* **2006**, *35*, 424−440.
(92) Lide, D. R. *CRC Handbook of Chemistry and Physics*, 82nd ed.; Taylor & Francis, 2002.
(93) Parthey, M.; Gluyas, J. B. G.; Fox, M. A.; Low, P. J.; Kaupp, M. *Chem.—Eur. J.* **2014**, *20*, 6895−6908.
(94) Demadis, K. D.; Hartshorn, C. M.; Meyer, T. J. *Chem. Rev.* **2001**, *101*, 2655−2686.
(95) Brunschwig, B. S.; Creutz, C.; Sutin, N. *Chem. Soc. Rev.* **2002**, *31*, 168−184.
(96) Nelsen, S. F. *Chem.—Eur. J.* **2000**, *6*, 581−588.
(97) Atwood, C. G.; Geiger, W. E. *J. Am. Chem. Soc.* **2000**, *122*, 5477−5485.
(98) Maurer, J.; Sarkar, B.; Schwederski, B.; Kaim, W.; Winter, R. F.; Záliš, S. *Organometallics* **2006**, *25*, 3701−3712.
(99) Fox, M. A.; Roberts, R. L.; Khairul, W. M.; Hartl, F.; Low, P. J. *J. Organomet. Chem.* **2007**, *692*, 3277−3290.
(100) Linseis, M.; Záliš, S.; Zabel, M.; Winter, R. F. *J. Am. Chem. Soc.* **2012**, *134*, 16671−16692.
(101) Dong, T. Y.; Hendrickson, D. N.; Pierpont, C. G.; Moore, M. F. *J. Am. Chem. Soc.* **1986**, *108*, 963−971.
(102) Renz, M.; Theilacker, K.; Lambert, C.; Kaupp, M. *J. Am. Chem. Soc.* **2009**, *131*, 16292−16302.
(103) Kundu, T.; Schweinfurth, D.; Sarkar, B.; Mondal, T. K.; Fiedler, J.; Mobin, S. M.; Puranik, V. G.; Kaim, W.; Lahiri, G. K. *Dalton Trans.* **2012**, *41*, 13429−13440.
(104) Wadman, S. H.; Havenith, R. W. A.; Hartl, F.; Lutz, M.; Spek, A. L.; van Klink, G. P. M.; van Koten, G. *Inorg. Chem.* **2009**, *48*, 5685−5696.
(105) Mays, M. J.; Sears, P. L. *J. Chem. Soc., Dalton Trans.* **1973**, 1873−1875.
(106) Shaw, A. P.; Ryland, B. L.; Norton, J. R.; Buccella, D.; Moscatelli, A. *Inorg. Chem.* **2007**, *46*, 5805−5812.
(107) Wanandi, P. W.; Tilley, T. D. *Organometallics* **1997**, *16*, 4299−4313.
(108) LeSuer, R. J.; Buttolph, C.; Geiger, W. E. *Anal. Chem.* **2004**, *76*, 6395−6401.
(109) Fourie, E.; Swarts, J. C.; Lorcy, D.; Bellec, N. *Inorg. Chem.* **2010**, *49*, 952−959.

DOI: 10.1021/acs.organomet.5b00104
Organometallics XXXX, XXX, XXX−XXX

(110) Swarts, J. C.; Nafady, A.; Roudebush, J. H.; Trupia, S.; Geiger, W. E. *Inorg. Chem.* **2009**, *48*, 2156−2165.
(111) Nemykin, V. N.; Rohde, G. T.; Barrett, C. D.; Hadt, R. G.; Bizzarri, C.; Galloni, P.; Floris, B.; Nowik, I.; Herber, R. H.; Marrani, A. G.; Zanoni, R.; Loim, N. M. *J. Am. Chem. Soc.* **2009**, *131*, 14969−14978.
(112) Miyaura, N.; Suzuki, A. *Org. Synth.* **1990**, *68*, 130−132.
(113) Sheldrick, G. M. *Acta Crystallogr., Sect. A* **1990**, *46*, 467−473.
(114) Sheldrick, G. M. *Program for Crystal Structure Refinement*; Universität Göttingen: Göttingen, Germany, 1997.
(115) Farrugia, L. J. *J. Appl. Crystallogr.* **2012**, *45*, 849−854.
(116) Noviandri, I.; Brown, K. N.; Fleming, D. S.; Gulyas, P. T.; Lay, P. A.; Masters, A. F.; Phillips, L. *J. Phys.Chem. B* **1999**, *103*, 6713−6722.
(117) Ruiz, J.; Daniel, M.-C.; Astruc, D. *Can. J. Chem.* **2006**, *84*, 288−299.
(118) Nafady, A.; Geiger, W. E. *Organometallics* **2008**, 5624−5631.
(119) Dunsch, L.; Petr, A. *Ber. Bunsenges. Phys. Chem.* **1993**, *97*, 436−439.
(120) Petr, A.; Dunsch, L.; Neudeck, A. *J. Electroanal. Chem.* **1996**, *412*, 153−158.
(121) Haubner, K.; Tarábek, J.; Ziegs, F.; Lukeš, V.; Jaehne, E.; Dunsch, L. *J. Phys. Chem. A* **2010**, *114*, 11545−11551.
(122) Perdew, J. P.; Burke, K.; Ernzerhof, M. *Phys. Rev. Lett.* **1996**, *77*, 3865−3868.
(123) Laikov, D. N.; Ustynuk, Y. A. *Russ. Chem. Bull.* **2005**, *54*, 820−826.
(124) Laikov, D. N. *Chem. Phys. Lett.* **1997**, *281*, 151−156.
(125) Neese, F. *WIRes. Comput. Mol. Sci.* **2012**, *2*, 73−78.
(126) Neese, F.; Wennmohs, F.; Hansen, A.; Becker, U. *Chem. Phys.* **2009**, *356*, 98−109.
(127) Neese, F. *J. Chem. Phys.* **2005**, *122*, 34107.
(128) Van Wüllen, C. *J. Chem. Phys.* **1998**, *109*, 392−399.
(129) Pantazis, D. A.; Chen, X.-Y.; Landis, C. R.; Neese, F. *J. Chem. Theory Comput.* **2008**, *4*, 908−919.

DOI: 10.1021/acs.organomet.5b00104
Organometallics XXXX, XXX, XXX−XXX